UNIVERSIDAD DE COSTA RICA
SISTEMA DE ESTUDIOS DE POSGRADO

IMPACT OF RAINFALL ON THE DIURNAL CYCLE OF SURFACE FLUXES IN A COFFEE PLANTATION

Tesis sometida a consideración de la Comisión del Programa de Estudios de Posgrado en Ciencias de la Atmósfera para optar por el grado y título de Maestría Académica en Ciencias de la Atmósfera

ROSANGÉLICA MONTERO ACUÑA

Ciudad Universitaria Rodrigo Facio, Costa Rica

2022

Dedication and acknowledgements

I want to dedicate this thesis first of all to God, who guides and accompanies me at all times, to my boyfriend Luis Angel for his support and unconditional love at all times and to my family, my parents and siblings, for always being there.

I thank Finca la Hilda and all those who have contributed to this research: Fabio Badruit Agricultural Experimental Station, CICA, CIGEFI, LOSIC, Raquel Ramírez, Federico Montero, MSc. Juan José Leitón, Cristina Chinchilla, Mayela Monge, José Miguel Araya, Eddy and Cristian.

I thank in a very special way, my tutor, the PhD. Ana María Durán, for her accompaniment throughout this process and all these years, for her valuable contribution and feedback to this research and to my professional career.

Likewise, I thank the readers, PhD. Marco Gutiérrez and PhD. Mark Johnson for every contribution during this investigation.

Esta Tesis fue aceptada por la Comisión del Programa de Estudios de Posgrado en Ciencias de la Atmósfera de la Universidad de Costa Rica, como requisito parcial para optar al grado y título de Maestría Académica en Ciencias de la Atmósfera.

Dr. Erick Rivera Fernández
Representante de la Decana
Sistema de Estudios de Posgrado

Dra. Ana María Durán Quesada
Directora de tesis

Dr. Mark S. Johnson
Asesor

Dr. Marco Gutiérrez Soto
Asesor

Dr. Rodrigo Castillo Rodríguez
Director del Programa de Posgrado

Rosangélica Montero Acuña
Sustentante

Contents

Resumen

Actualmente los estudios sobre el impacto de extremos de precipitación en actividades agrícolas están enfocados principalmente en sequía, sin embargo, el análisis del posible impacto de eventos fuertes de lluvia es necesario, ya que, los cultivos son altamente vulnerables a la disponibilidad de agua y cambios en la duración e intensidad de los periodos de lluvia. En este caso, el análisis se lleva a cabo en una plantación de café ("Finca La Hilda"), en la provincia de Alajuela, Costa Rica. La región en que se localiza La Hilda se caracteriza por ser parte del régimen Pacífico de precipitación, el cual se ve modulado por fenómenos tanto a escala local como a escala regional (Zona de convergencia Intertropical, ZCIT) e intra-estacional (El Niño Oscilación del Sur, ENOS). Se analiza la influencia de los eventos de mayor intensidad de lluvia y su influencia con los flujos de masa y energía, medidos mediante la técnica Covarianza de Torbellinos. Para seleccionar los eventos, se utiliza la categorización de Mukherjee y se utilizan los días de lluvia que caen en las categorías moderadamente fuerte, fuerte y muy fuerte. La categorización de Mukherjee fue evaluada utilizando la técnica de percentiles, y se determinó su uso debido a que el registro observacional de La Hilda no permite realizar la clasificación de eventos con base en la climatología debido a la extensión temporal del registro. Asimismo, se indagó sobre los modulares de cada uno de estos eventos, concluyendo que la ZCIT y ondas tropicales, son los principales precursores de eventos de fuerte intensidad en La Hilda. Los flujos de CO_2, LE (calor latente) y H (calor sensible) presentaron una variabilidad marcada tanto para cada estación de año (estación seca, primera parte de la estación lluviosa, Veranillo (MSD), segunda parte de la estación lluviosa), como para cada evento de precipitación. La lluvia estuvo relacionada con el comportamiento de los flujos, siendo así, para los eventos de larga duración (Huracán Eta) se observó un comportamiento casi constante de los flujos de CO_2 y LE y una variabilidad bastante marcada para H. Otras variables estudiadas son la eficiencia en el uso del agua (WUE, siglas en inglés), flujo de savia y contenido de humedad del suelo (SWC, siglas en inglés). Los tres mostraron ser influenciados por eventos fuertes de precipitación. El WUE mostró menores valores en la época seca comparado a la época lluviosa y hubo un mayor flujo de savia para los eventos más fuertes de precipitación, sin incluir el huracán Eta.

Abstract

Currently, studies on the impact of precipitation extremes on agricultural activities are mainly focused on drought, however, the analysis of the possible impact of heavy rain events is necessary, since crops are vulnerable to water availability. In this case, the analysis is carried out in a coffee plantation ("Finca La Hilda"), in the province of Alajuela, Costa Rica. This region is characterized by being part of the Pacific precipitation regime, which is modulated by phenomena both at a local scale and at a regional scale (Intertropical Convergence Zone, ITCZ) and intraseasonal variability (El Niño Southern Oscillation, ENSO). The influence of the events of greater intensity of rainfall and its influence with the fluxes of mass and energy, measured by the Eddy Covariance technique, was analyzed. To choose the events, the categorization of Mukherjee and the rainy days that fall in the moderately heavy, heavy and very heavy categories were used. The Mukherjee classification was evaluated for the site using percentiles for the available meteorological record and selected due to the length of the site record is not sufficient for climatological based analysis. The modulators of each of these events were investigated, concluding that the ITCZ and tropical waves are the main precursors of high intensity events in La Hilda. The fluxes of CO_2, LE and H presented a marked variability both for each season of the year (dry season, first part of the rainy season, Mid-Summer Drought (MSD), second part of the rainy season), and for each precipitation event. In both cases, the rainfall was related to the behavior of the fluxes, thus, for long-duration events (Hurricane Eta) an almost constant behavior of the CO_2 and LE fluxes were observed, and a quite marked variability for H. Other variables studied were water use efficiency (WUE), sap flow, and soil water content (SWC). All three showed to be influenced by strong precipitation events. The WUE, as expected, showed lower values in the dry season compared to the rainy season and there was a higher sap flow for the strongest precipitation events, not including Hurricane Eta.

Table list

Figures

UNIVERSIDAD DE COSTA RICA

SEP Sistema de Estudios de Posgrado

Autorización para digitalización y comunicación pública de Trabajos Finales de Graduación del Sistema de Estudios de Posgrado en el Repositorio Institucional de la Universidad de Costa Rica.

Yo, Rosangélica Montero Acuña, con cédula de identidad 402230167, en mi condición de autor del TFG titulado IMPACT OF RAINFALL ON THE DIURNAL CYCLE OF SURFACE FLUXES IN A COFFEE PLANTATION

Autorizo a la Universidad de Costa Rica para digitalizar y hacer divulgación pública de forma gratuita de dicho TFG a través del Repositorio Institucional u otro medio electrónico, para ser puesto a disposición del público según lo que establezca el Sistema de Estudios de Posgrado. **SI** [X] **NO** *[ ]

***En caso de la negativa favor indicar el tiempo de restricción:_____año (s).**

Este Trabajo Final de Graduación será publicado en formato PDF, o en el formato que en el momento se establezca, de tal forma que el acceso al mismo sea libre, con el fin de permitir la consulta e impresión, pero no su modificación.

Manifiesto que mi Trabajo Final de Graduación fue debidamente subido al sistema digital Kerwá y su contenido corresponde al documento original que sirvió para la obtención de mi título, y que su información no infringe ni violenta ningún derecho a terceros. El TFG además cuenta con el visto bueno de mi Director (a) de Tesis o Tutor (a) y cumplió con lo establecido en la revisión del Formato por parte del Sistema de Estudios de Posgrado.

ROSANGELICA MONTERO ACUÑA (FIRMA)

Firmado digitalmente por ROSANGELICA MONTERO ACUÑA (FIRMA)
Fecha: 2022.12.10 08:45:11 -06'00'

FIRMA ESTUDIANTE

Nota: El presente documento constituye una declaración jurada, cuyos alcances aseguran a la Universidad, que su contenido sea tomado como cierto. Su importancia radica en que permite abreviar procedimientos administrativos, y al mismo tiempo genera una responsabilidad legal para que quien declare contrario a la verdad de lo que manifiesta, puede como consecuencia, enfrentar un proceso penal por delito de perjurio, tipificado en el artículo 318 de nuestro Código Penal. Lo anterior implica que el estudiante se vea forzado a realizar su mayor esfuerzo para que no sólo incluya información veraz en la Licencia de Publicación, sino que también realice diligentemente la gestión de subir el documento correcto en la plataforma digital Kerwá.

1. Introduction

The distribution of precipitation over Costa Rica is characterized by the Pacific regime with a well-defined dry and rainy season and a Caribbean regime that features rainfall all year. For the Pacific regime, the rainy season runs from May to November, the rainiest months are September and October, with rainfall occurring predominantly in the afternoon and early evening. The dry season runs from December to March, the driest and warmest month is March, and April is considered a transition month. The Pacific regime is characterized by a bimodal distribution with a dry period in the middle of the rainy season, in July or August, known as Mid-Summer Drought (MSD, Magaña et al., 1999). The MSD is not a true drought, but rather is characterized by a reduction in precipitation between the first and second legs of the rainy season. The early appearance of the MSD can affect crops at a critical stage of its development, especially for rainfed crops where the only moisture supply is rainwater or, conversely, if the MSD is prolonged for a long time, the deficiency of moisture in the soil makes it necessary to apply irrigation (Ramírez, 1983).

The Caribbean precipitation regime does not exhibit a defined dry season and rainfall events occur all year with ranges between 100 mm and 200 mm. Rainfall under the Caribbean regime has a maximum in July, contrasting with the rainfall minimum during the MSD in the regions of Pacific influence (IMN, 2020). The regional precipitation patterns are driven by moisture transport from the Caribbean Sea, with the Caribbean Low-Level Jet (CLLJ) as the main conveyor of regional moisture (Durán-Quesada et al., 2010; 2017). It has been suggested that the first leg of the rainy season (May to June) has a strong influence from local processes and surface-atmosphere feedback interactions, with surface fluxes and orography playing an important role for rainfall occurrence, while large scale drivers of regional precipitation include the seasonal migration of the Intertropical Convergence Zone (ITCZ), deep convection, low-level moisture transport, cyclone activity and mid-latitude air intrusions (Durán-Quesada et al., 2020).

Variability of rainfall in Costa Rica is modulated by modes like El Niño-Southern Oscillation (ENSO, Ahrens & Henson, 2009) and the Madden Julian Oscillation (MJO, Holton, 2004) at interannual and intra-seasonal timescales respectively. ENSO is the dominant interannual variability mode affecting moisture supply in Central America and exerts a strong forcing on rainfall amount and spatial distribution (Duran-Quesada et al., 2017). The impact of ENSO is variable as the intensity of the phenomenon determines the way it affects the region (Ahrens & Henson, 2009). During a very strong warm ENSO event, precipitation under the Pacific regime tends to be below average (IMN, 2021a); when rainfall deficit is sustained a drought develops and impacts the regional ecosystems (Cooley et al., 2019; Hidalgo et al, 2019). The number, intensity and positioning of the tropical cyclones is largely variable depending on the ENSO phase (Durán-Quesada et al., 2020). During warm ENSO events, the potential formation of tropical cyclones is low (Ahrens & Henson, 2009, IMN, 2021a) which contributes to the reduction in precipitation.

While the signal for drought is dominated by internal variability, Pascale et al., (2021) shows that climate change also influences the severity of drought in the region. While warming trends have been well documented for the region (Stewart et al., 2022), the assessment of precipitation trends due to anthropogenic climate change is hindered by lack of long-term records (Allan et al., 2021). Observational limitations also affect the validation of future climate scenarios derived from global and regional circulation models, adding uncertainty to the available tools to analyze how climate change may impact human activities, including food security and the occurrence of extreme precipitation events. Because the impact of precipitation extremes on agricultural activities is often focused on drought and its impacts on productivity, the case of heavy rainfall events is understudied. To understand further impacts of climate change due to warming on crops, it is important to improve the understanding of the relationships between water and plants under heavy rainfall conditions. Water balance is the most physiographic characteristic of any territory, it determines its typical landscapes, climate features, land use and possible water management. The water balance components are precipitation, evapotranspiration (ET) and runoff (Shiklomanov, 2009).

ET represents the latent heat flux (LE) between surface and atmosphere, which quantifies the relationship between the water balance components and the surface fluxes and is related with the energy balance (Xiao et al., 2013; Lal, 2004). Changes in frequency and magnitude of rainfall events induce changes in the variability of soil water content (SWC) and interact with the carbon cycling (Harper et al. 2005). Wu et al. (2013) showed that precipitation variability is one of the most important climate factors that can affect the gross primary production (GPP) variability, that is the CO_2 assimilated by the plants during photosynthesis (Cabral et al., 2013). An increase in the number of periods of precipitation will also result in low radiation which reduces the monthly GPP. In North America, Huxman et al. (2004) determined a relationship between the pulse size of precipitation and the infiltration depth. They noticed that if pulse size of rainfall increases in such a way water infiltrates to a greater depth and persists for sufficient time to stimulate plant water, ecosystem photosynthesis eventually increases, on the contrary, small, shallowly infiltrating storms primarily increase microbial respiration. Thus, high respiration rates from biological processes can occur quickly following a precipitation pulse resulting in substantial CO_2 release to the atmosphere.

Rainfall and ET are connected through the hydrological cycle because a fraction of the water transported from the surface to the atmosphere is later precipitated (Kleidon, 2018). ET is a very important component of the water balance in agricultural areas, as well as a great consumer of available solar energy, especially in irrigated agricultural areas, as it consumes 60%–80% of the net radiation during the crop-growing seasons (Timm et al. 2014). According to Wei & Dirmeyer (2019), the water vapor for rainfall comes from local and nonlocal surface evaporation, despite rainfall being more sensitive to local than nonlocal evaporation. They found that in 65% of total land areas, precipitation is more sensitive to local ET, and only about a third of land areas were more sensitive to non-local ET. ET is associated with annual precipitation, GPP, growing season length of the vegetation and latitude, being in the tropical and subtropical sites the highest values of ET (Xiao et al., 2013). In general, the large variability of annual ET across vegetation types can be attributed to mean annual climate conditions, plant functional types and water supply as higher precipitation may imply larger ET (Xiao et al., 2013).

Full-sun (FS) coffee plantations has gradually become a more common cultivation system over the last 30 years, especially in the most favorable areas of Central America, where it has been found that, coffee transpired more per unit leaf area in FS than under shade (agroforestry, AF), an indication of higher environmental coffee stress in non-shaded conditions (Peters and Samper, 2001; Van Kanten & Vaast, 2006). De Carvalho Gomes et al. (2016) studied the relation between full-sun (FS) and agroforestry (AF) coffee plantations. They found that soil CO_2 flux variability during the day decreases with increasing canopy cover and that the flux is more stable in AF systems, showing less diurnal variation from morning to midday than in FS systems. This behavior in AF suggests that soil CO_2 flux is mainly due to heterotrophic soil respiration (soil microorganisms), rather than autotrophic respiration (roots). Thus, AFs resemble natural forests, with trees creating a soil microclimate that is suitable for the growth of soil microorganisms. In contrast, FS systems are subject to more stress on autotrophic and heterotrophic soil respiration due to higher soil temperature at noon. As the vegetation cover regulates local soil temperature and moisture, it becomes a major driver of soil CO_2 flux dynamics.

The influence of precipitation on crops is a much more complex issue than the assessment of precipitation variability. Furthermore, crop-precipitation relationships involve processes at local scales that are often neglected in the traditional regional studies and that are misrepresented in regional climate models. To improve our knowledge on crop-precipitation relationships and leverage that information to contribute to better interpretations of future climate scenarios, a detailed analysis of the different time scales of precipitation, plant responses as well as the surface energy and mass fluxes are needed.

The main objective of this investigation was to quantify the response of the plant-water relationships to the seasonality of rainfall in agroclimatic zones of Pacific influence. This quantification was carried out through the analysis of three specific objectives: study the impact of rainfall intensity on surface fluxes based on a full agrometeorological experimental setup in the coffee farm "Finca La Hilda", located in Poás of Alajuela in Costa Rica under optimal production conditions. Investigate the response of evapotranspiration and CO_2 flux to rainfall intensity. Evaluate the impact of heavy rainfall

in the water use efficiency in the system. With this, a climatological characterization of the study area is presented along with the annual cycle of the surface fluxes and the response of the surface fluxes based on different precipitation intensities is studied to explore how low to very heavy rainfall regimes affect the behavior of the surface fluxes in a FS system.

2. Data and Methods

2.1 Characteristics of the coffee

Coffee (*Coffea arabica L.*) originates from the Ethiopian tropical forests, with a latitude between 6-9° North and an altitude between 1600-2800 m.a.s.l. (Van Kanten & Vaast, 2006). Coffee is sensitive to excessive heat or cold or to sudden changes in temperature, therefore, it requires certain conditions for healthy and satisfactory growth, including a temperature range between 15° C and 24° C, with a well-distributed annual rainfall (1500-2500 mm) and a dry season of 2-3 months (Nair, 2010; Van Kanten & Vaast, 2006). Likewise, *Coffea arabica* is a perennial woody brush with a complex phenological cycle, that is, the flowering and fruiting phases (vegetative and reproductive phases) occur in a two-year cycle, with the vegetative and floral stages occurring in the first year and fruit production in the next characterizing the species as biannual, unlike other species that complete their phenological cycle in the same year (Torres et al., 2021).

Coffee is a C_3 plant, this type of plant fixes CO_2 during the day via Rubisco, when its stomata are open. During the Calvin cycle, CO_2 combines with a 5-carbon sugar (RuBP) to form a 6-carbon compound that transforms into 3 molecules. Then, in the reductive phase, the 6 of 3-PGA molecules are converted by two reactions into 6 of 3-phosphoglyceraldehyde (G3P) molecules. Finally, one of these six molecules is used in the manufacture of carbohydrates and the other five are used to resynthesize three RuBP molecules. The main limitation of this process is photorespiration, it occurs when the Rubisco fixes O_2 instead of CO_2, as CO_2 begins to become scarce within leaf spaces, Rubisco adds O_2 to the Calvin Cycle. The product is cleaved, and a two-carbon compound leaves the chloroplast. The drawback is that in addition to the loss of carbon already fixed, energy is wasted, and no sugar is produced (Campbell & Reece, 2007; Mares, 2017; Wilfred, 2008).

2.2 Data and experimental set up

A coffee plantation located in La Hilda, in the canton of Poás in the province of Alajuela was the study site for this research. The experimental site is a plot in La Hilda, a 30-year-old coffee plantation which was renewed by full pruning in 2015, it is located in the Pacific regime influence area at a height between 1000 and 1500 m.a.s.l with predominant Andosols as soil type (Figure 2.1). The monitoring site used for this analysis is a FS system, located in a 6.9 ha. field with the Sarchimor T5296 coffee (arabica coffee variety). The meteorological conditions for the analysis region were analyzed considering two nearby automatic weather stations (AWS) because no long-term observations were available on the site to construct the climatology. A Campbell AWS in Fraijanes town of Alajuela province (1500-1700 m.a.s.l.), within a 12 km radius from La Hilda, corresponds to the nearest station from the National Meteorological Institute (IMN, Spanish acronym) network with long-term records (1980-2021) A complementary Davis AWS located at La Hilda with records from 2009 was also used for comparison of conditions with the nearest station climatology (Figure 2.1). Hourly frequency was used.

2.2.1 Eddy Covariance technique

A closed path Eddy Covariance (EC) system (LI-COR Li-7200RS) was deployed in the FS in December 2019 as part of the experimental arrangement to monitoring surface energy, CO_2 and water vapor fluxes of the CFlux project (Chinchilla et al., 2021, Figure 2.1**,** Figure 2.2). The Li-7200RS deployed includes an infrared gas analyzer (IRGA) that responds to the attenuation (by absorption) of an infrared light bean (Lee et al., 2004). The closed path system measures air that has been drawn through some distance of tubing before reaching the analyzer, the closed path system was selected due to the influence of rainfall for the site, which also enabled the use of the information to assess the impact of rainfall on the fluxes. The system integrates a sonic anemometer that measures the 3-dimensional components of the wind and a full Biomet system which integrates a series of meteorological and soil sensors as listed in Table 2.1. In the IRGAS, gas densities are calculated from the ratio of the absorbed radiation to a reference value. The dry mole fractions of CO_2 and H_2O in the air sample are estimated as moles of gas per mole of dry

air that explains changes in air density due to H_2O content, pressure, and temperature of the air sample (Li-Cor, 2016b; Li-Cor, 2020). The correspondent data quality control process was carried out and final data was processed using the TOVI software (LI-COR Biosciences, Lincoln, NE USA).

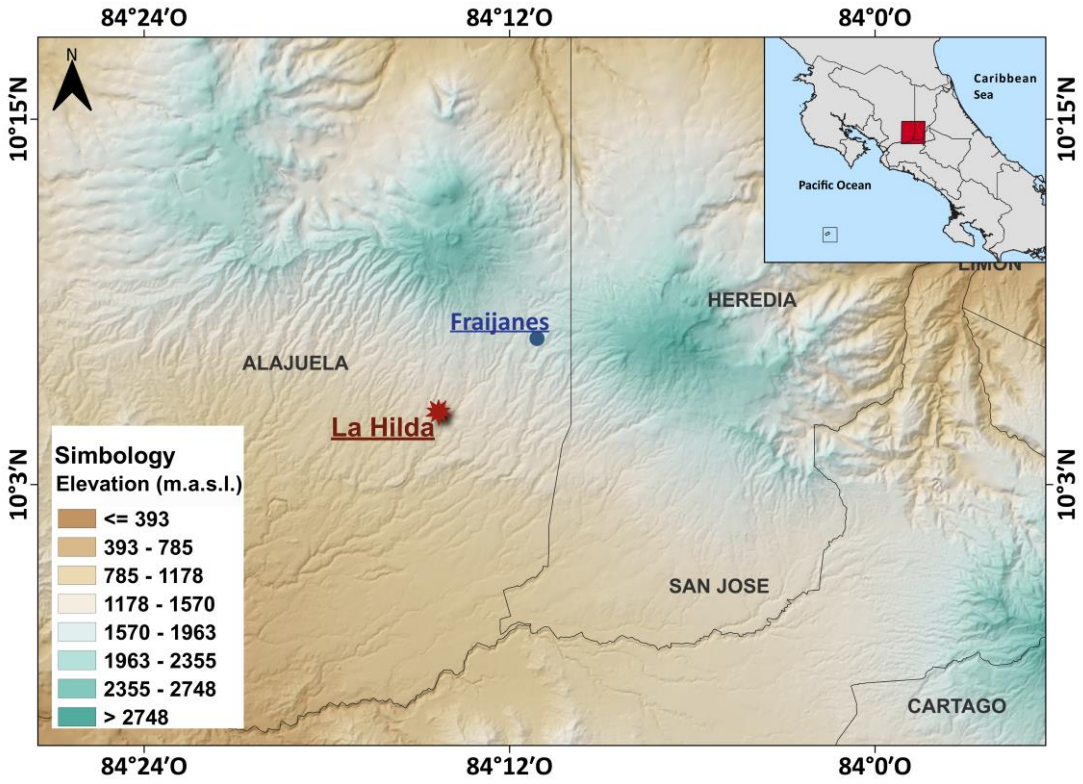

Figure 2.1 *Location of the meteorological stations and the EC system used: La Hilda at altitude between 1000- 1500 m.a.s.l. (10.0893´´N, 84.235088´´W) and Fraijanes at altitude between 1500 and 1900 m.a.s.l. (10.1300´´N, 84.180000´´W).*

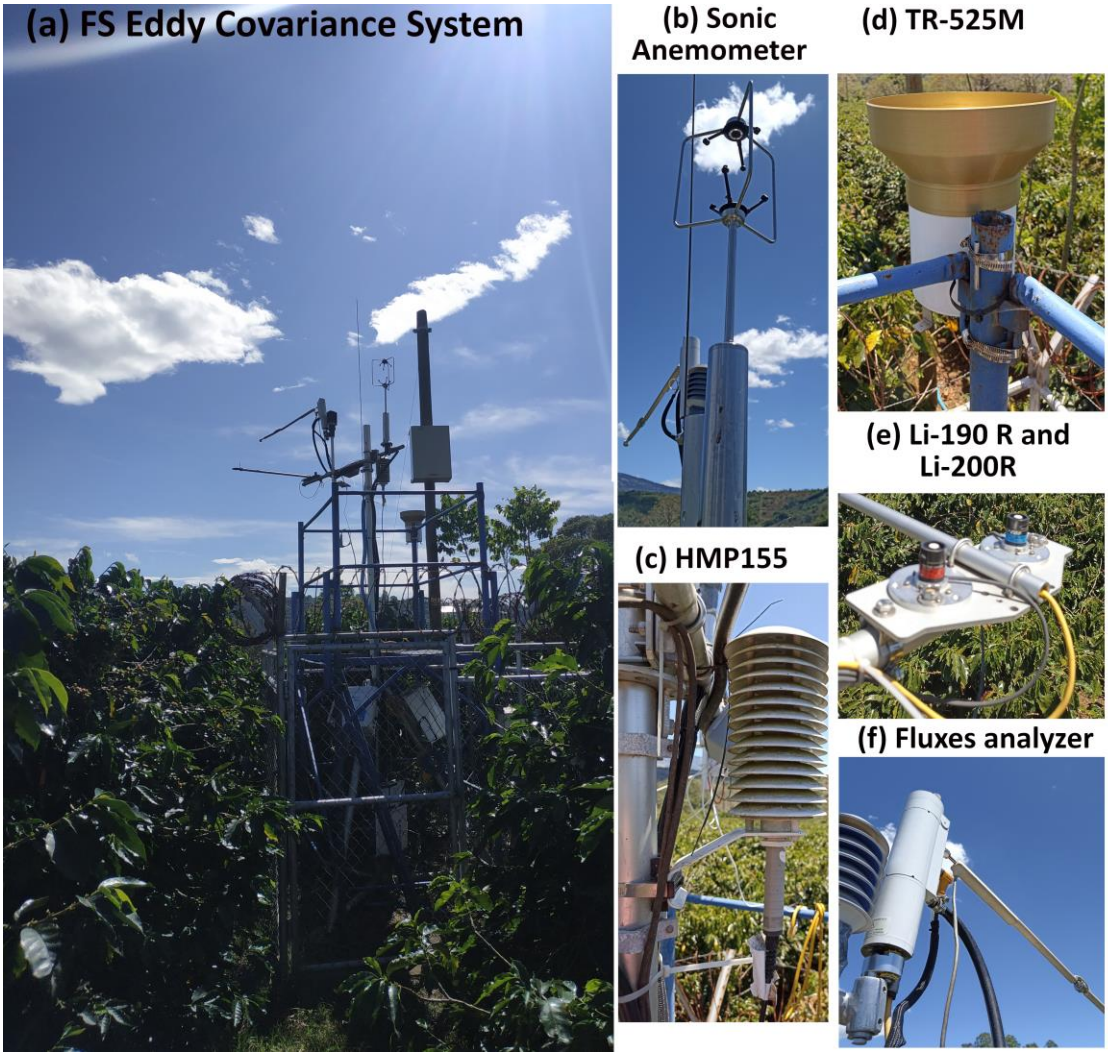

Figure 2.2 *(a) Li-7200RS Eddy Covariance full-sun system on coffee plantation at La Hilda. Sensors used by the EC to measure different variables (*Table 2.1*): (b)sonic anemometer, (c) humidity and temperature probe, (d) rain gauge, (e) line quantum sensor and pyranometer and (f) fluxes analyzer.*

Sensor	***Description***
Li-190R Line Quantum Sensor	It is designed to measure photosynthetically active radiation (PAR) in applications where the radiation to be measured is spatially non-uniform, such as within plant canopies. The sensor output is a current (µA) signal that is directly proportional to hemispherical PAR. A multiplier is used to convert the current signal into units of radiation (µmol s-1 m-2) (Li-Cor, 2019b).
Li-200R Pyranometer	It measures global solar radiation and should only be used to measure unobstructed day light. The sensor output is a current (µA) signal that is directly proportional to hemispherical solar radiation.

	A multiplier is used to convert the current signal into units of radiation (Wm-2) (Li-Cor, 2019a).
HMP155 Humidity and Temperature Probe	It provides reliable humidity and temperature measurement. With its fast response time, the additional temperature probe is ideal for measurement in environments with changing temperatures. The humidity range is from 0-100% and the temperature range is from -80 - 60 °C (Vaisala, 2012).
TR-525M Tipping Bucket Rain Gauge	It has a resolution of 0.1 mm. It contains an open top, which allows rainfall to fall in the upper portion, which is called a collector. The collected water is funneled to a mechanical device (Tipping Bucket), which incrementally measures the accumulation of rain and causes a momentary closure of a switch. As water is collected, the tipping bucket fills to the point where it tips over (Texas Electronics, 2017).
CNR4 Net Radiometer	It measures the energy balance between incoming short-wave and long-wave Far Infrared (FIR) radiation versus surface-reflected short-wave and outgoing long-wave radiation. It consists of a pyranometer pair, one facing upward, the other facing downward, and a pyrgeometer pair in a similar configuration. The pyranometer pair measures the short-wave radiation. And the pyrgeometer pair measures long-wave radiation. The most common application is the measurement of Net (total) Radiation at the earth's surface (Kipp & Zonen; 2014).
HFP01 Soil Heat Flux Plates	It outputs a voltage signal that is proportional to the heat flux of the surrounding medium (usually soil). It is typically used for energy-balance or Bowen-ratio flux systems. At least two sensors are required for each site to provide spatial averaging (Campbell Scientific, 2012).
Hydraprobe soil Stevens	This sensor measures soil temperature, soil moisture, dielectric permittivity and soil electrical conductivity. It takes into account the energy storage and energy loss across the soil area using a 50MHz radio frequency wave. Three main structural components to the HydraProbe: the marine grade stainless steel tine assembly is the wave guide. The base plate is 25 mm in diameter. Electromagnetic waves are transmitted and received by the center tine. The head or body of the probe contains the circuit boards, microprocessors, and all the other electrical components. The outer casing is ABS (Stevens, 2018).

Table 2.1 *Additional EC sensors for the measurement of different meteorological variables.*

2.3 Methodology

2.3.1 Climatology of rainfall and temperature

It is not possible to establish the regional climatology of temperature and rainfall for the site given the length of available records. Hence, long-term available information from Fraijanes was used as the La Hilda meteorological record is shorter (2009-2020) considering that Fraijanes is colder and located at higher elevation (Figure 2.1 and Figure 3.1). The comparison of rainfall and temperature for the common period of the stations (2009-2020) was conducted to identify differences in the diurnal cycle of precipitation and temperature, and accumulated rainfall. From hourly data, daily and monthly accumulated rainfall was computed, as well as daily and monthly averages for the maximum, minimum and mean temperatures, with the aim of analyzing the variability and behavior of these variables, for the subsequent study of energy and CO_2 fluxes according to the distribution of rain at La Hilda during the 2020-2021 period.

2.3.2 Classification of rain events

Daily accumulated rainfall was estimated, and rainfall was categorized as light, moderate, rather heavy, heavy, and very heavy rainfall following Mukherjee et al. (2015) classification (Table 2.2). Next, the days where the rain was classified as heavy and very heavy were chosen to analyze them as outstanding events of the study period (Table 3.1). To determine the main synoptic modulators of these events (tropical cyclones, Intertropical Convergence Zone (ITCZ), tropical waves, trade winds, MJO, others), synoptic charts provided by IMN were used. The precipitation categories calculated with the daily precipitation data from La Hilda weather station is presented in Table 2.3. As can be seen, each category was assigned a percentile. When comparing the classification of Mukherjee et al. (2015) (Table 2.2) with the one calculated from percentiles (Table 2.3), differences were found between the categories, however, since in this research we focused mainly on the heavy and very heavy categories, the chosen events are part of the very heavy category in the calculation of percentiles, that is, they are outstanding events in both classifications.

Classification of rainfall	Daily Rainfall (R, mm d^{-1})
Light	$0.0 < R \leq 10.0$
Moderate	$10.0 < R \leq 35.5$
Rather heavy	$35.5 < R \leq 64.4$
Heavy	$64.4 < R \leq 124.4$
Very heavy	$R > 124.4$

Table 2.2 *Categorization of precipitation based on Mukherjee et al. 2015. This classification is based on daily accumulated rainfall and has five classes: light, moderate, rather heavy, heavy and very heavy divided into different ranges of daily rainfall.*

Month	Moderate (Percentile 80)	Rather heavy (Percentile 90)	Heavy (Percentile 95)	Very heavy (Percentile 99)
1	0.0	0.3	0.8	3.6
2	0.0	0.0	0.4	5.4
3	0.0	0.0	0.3	8.3
4	4.6	15.6	27.8	47.2
5	22.8	35.4	49.7	85.9
6	20.4	32.8	43.3	80.7
7	10.6	25.0	42.5	64.0
8	18.2	35.8	49.6	83.4
9	29.2	42.8	59.1	89.9
10	25.8	40.2	53.8	82.7
11	6.3	23.2	39.7	100.6
12	0.4	1.8	4.8	36.1

Table 2.3 *Precipitation categories calculated from the 80th, 90th, 95th and 99th percentiles with La Hilda rainfall data for the entire period of the 2009-2021 season. The units of each column are mm/day and are divided into moderate, rather heavy, heavy and very heavy rainfall.*

2.3.3 Surface fluxes

The EC method allows the measurement of energy and mass transported by eddies, transport of energy and mass depends on the turbulent flow, which is calculated as $\overline{w'c'}$, where these two variables would be the fluctuating terms of the velocity component in the direction of motion (w) and the concentration of a dimensionless scalar magnitude (c),

such as temperature of the air for sensible heat, density of CO_2 for CO_2 flux and density of H_2O for H_2O flux (Burba & Anderson, 2010; Krishnan et al., 2012), the vertical flux can be represented as:

$$F = \overline{\rho_a w s} \tag{2.1}$$

Where ρ_a is the air density, w is the vertical velocity and s is the mixing ratio, which is defined as:

$$s = \frac{\rho_c}{\rho_a} \tag{2.2}$$

For s substance c in the air.

Therefore, the flux is equal the mean product of the air density, the vertical wind speed, and the mixing ratio of the tracer of interest. Applying the Reynolds decomposition, which is defined as a mean value plus a fluctuating value (Foken & Napo, 2008):

$$x = \bar{x} + x' \tag{2.3}$$

From the equation 2.1 and considering that the average deviation from the average is zero, we obtain:

$$F = \overline{\rho_a}\bar{w}\bar{s} + \overline{\rho_a}\overline{w's'} + \bar{w}\overline{\rho_a{}'s'} + \bar{s}\overline{\rho_a'w'} + \overline{\rho_a{}'s'w'} \tag{2.4}$$

For conventional EC it is supposed that fluctuations in air density are negligible, thus from equation 2.4 it is obtained

$$F = \overline{\rho_a}\bar{w}\bar{s} + \overline{\rho_a}\overline{w's'} \tag{2.5}$$

Another assumption is made, where for horizontal homogeneous terrain it is supposed that mean vertical flow is considered as negligible, the turbulent flux is obtained as:

$$F \approx \overline{\rho_a}\overline{w's'} \tag{2.6}$$

which is approximately equal to product of the mean air density and the mean covariance between instantaneous deviations in vertical wind speed and mixing ratio.

It is also assumed that measurements are done inside the boundary layer of interest, the flow is fully turbulent (most of the net vertical transfer is done by eddies and, terrain is

horizontal and uniform which it involves that the average of fluctuations air density fluctuations, flow convergence and divergence are negligible).

In addition, an appropriate footprint must be chosen for the measurements. Flux footprint is the area "seen" by the instrument at the tower and decreases with increased roughness. Some considerations that must be taken into account to have an adequate footprint: The location of the tower should represent the area of interest for the prevailing wind directions. For sensors, the rule of thumb is that the measurement height should be 100 times less than the desired search to avoid sampling outside the area of interest. The lowest location height should be above the roughness sublayer. The rule of thumb is that ideally the height of the instrument should be twice the height of the canopy. If the terrain is patchy, with scattered bushes or trees, the ratio may need to increase up to 5 times the canopy height (Burba & Anderson, 2010).

2.3.3.1 Data analysis of surface fluxes

From the 30 min, quality-controlled EC system output, CO_2, latent heat (LE) and sensible heat (H) fluxes, were used to analyze the average diurnal and annual cycles as well as to further evaluate the impact of heavy rainfall events on the surface fluxes at sub-daily scales. CO_2, LE, H and soil water content (SWC) were analyzed for the 2020-2021 period and classified according to rainfall categories in Table 2.1. Hourly averages of these CO_2, LE, H and SWC, were used to classify the fluxes by synoptic (or large scale) conditions of Table 3.1. For each month in which an event above 70 mm was recorded, the diurnal cycle of the entire month was calculated for later comparison with the diurnal cycle of each event (Table 3.1).

2.3.3.2 Sap Flux

The sap flux is measured with a Dynagage Sap Flux Sensor every 30 minutes (Figure 2.3). This sensor measures the amount of heat carried by the sap which is converted in real-time sap flux in grams per hour. Other features are: non-invasive, models to fit stem

diameter from 2-150 mm, no calibration required and ±10% accuracy typical (Dynamax, 2007).

The method use by this sensor is the stem heat balance (SHB), implemented by Sakuratani (1981) and corrected by Baker & Van Bavel (1987). In this method, the heat input from an external annular heater is kept constant and fluxes of heat out of the system are calculated from measured temperature gradients, enabling direct calculation of the mass flux rate water in the stem (Baker & Van Bavel, 1987). Baker & Van Bavel (1987) created a new gauge to correct two problems, first, the manganin wire uses to make the heaters was susceptible to corrosion and the fragility of the thermojunctions.

Figure 2.3 *(a) Installation of the sap sensor in coffee. (b) Sap sensor once installed and collecting data at La Hilda.*

2.2.4 Water use efficiency

Water use efficiency (WUE) is defined as the ratio between total biomass (CO_2 gain) and water loss (ET) by the plant (Sharma et al 2015). In other words, it is used to determine the efficiency of plants to fix CO_2, relative to the amount of water loss by transpiration (Bhatla & Lal, 2018). Therefore, WUE was estimated from the gross primary production (GPP, gCO_2/kgH_2O) and evapotranspiration (ET, mm/day) data derived from the EC

system. For the calculation of the WUE, the data were taken every 30 minutes of ET and GPP and the daily accumulations were calculated, from these accumulations, the definition of WUE is applied as the radius of GPP and ET (WUE = GPP/ET) (Sharma et al., 2015, Chinchilla et al., 2021). In this case, the data corresponding to the days of extreme events were extracted and finally the monthly average of all the data for the years 2020 and 2021 were calculated.

3. Meteorological conditions at La Hilda

3.1 Long term rainfall and temperature averages

The annual cycle of precipitation at La Hilda and Fraijanes features well-defined dry and rainy seasons (Figure 3.1a and b). The annual precipitation at La Hilda is approximately 2300 mm while for Fraijanes it is approximately 3000 mm. The dry season goes from December to April and the rainy season goes from May to November, a decrease in precipitation is observed between July and August due to the influence of the MSD given the site is influenced by the Pacific precipitation regime. At La Hilda, the driest month is January (< 10 mm/month) while precipitation is maximum, on average, during September and October (> 400 mm/month). Based on exploration of the coffee trees during field visits, it is suggested that local moisture availability during December and early January is mostly associated with the presence of dew over the canopy. The first and second legs of the rainy season show that the second leg of the rainy season dominates the annual precipitation. In the case of Fraijanes this feature is more pronounced and a relevant difference between Fraijanes and La Hilda reflects that La Hilda has an even more marked dry season compared to higher altitude Fraijanes. Year to year rainfall variability is shown in Figure 3.1 (e and f), from which variations with drier and wetter intervals are observed. Precipitation variability at interannual scales is modulated by ENSO, with warm ENSO associated with drier conditions (Maldonado et. al 2018).

The distribution of maximum, minimum and mean temperature is represented with red, blue, and black, respectively (Figure 3.1c and d). The mean annual temperature at La Hilda is 20.4 °C, the warmest month is April with an annual mean maximum temperature of 21.8°C and the coldest month is October with an annual mean minimum temperature of 19.4°C. At Fraijanes the maximum temperature is 22°C and, the minimum temperature is 12°C. Fraijanes is the region with the lowest temperatures given this station is located at the highest altitude (Figure 2.1). The month with the maximum temperature in both stations is April, and the month with the minimum temperature is October at La Hilda and January for Fraijanes.

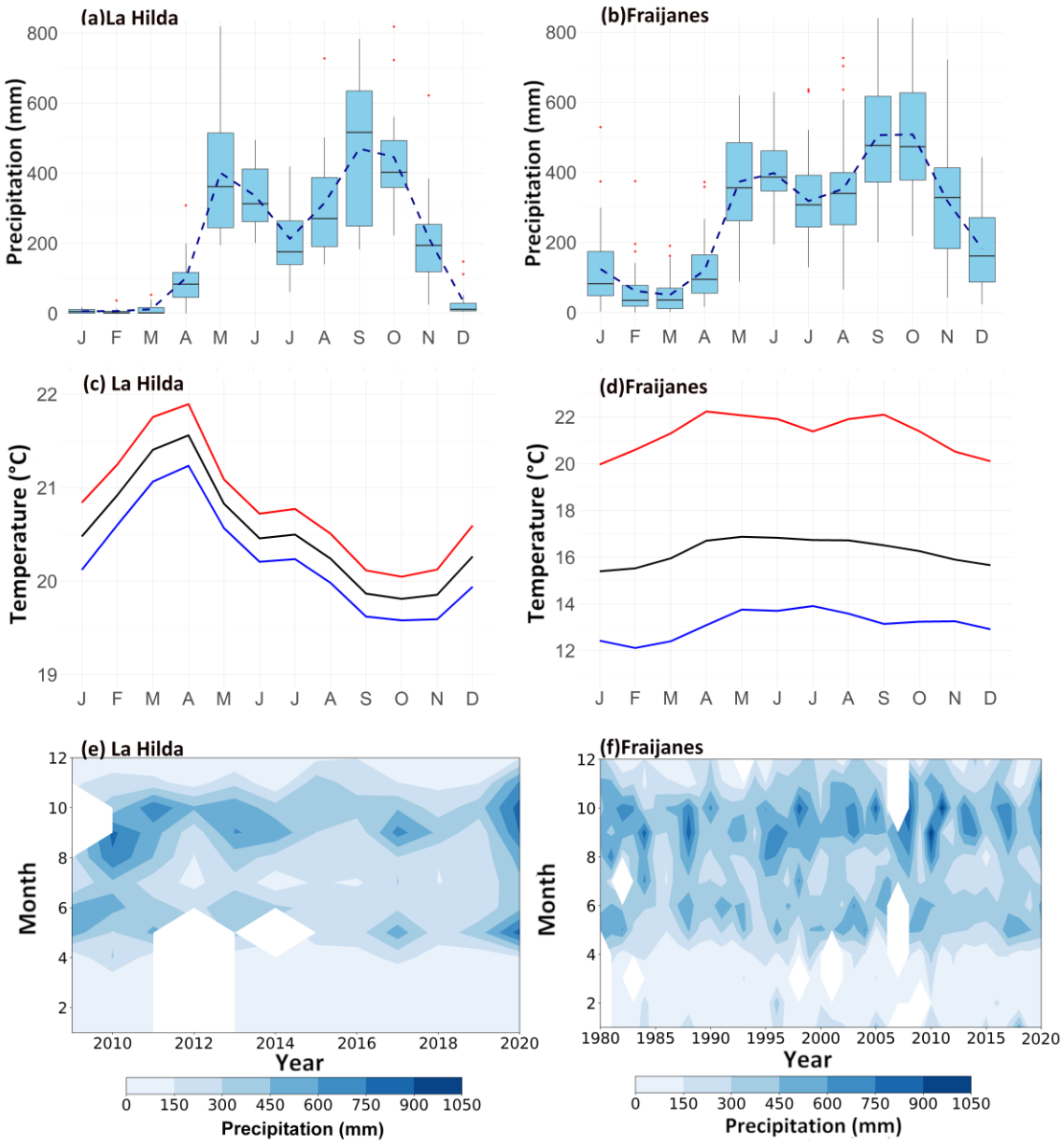

Figure 3.1 *(a) and (b) Monthly distribution of precipitation represented by boxes and the mean accumulated (dotted line blue). (c) and (d) Maximum, minimum and mean temperature, lines red, blue, and black, respectively. (e) and (f) Monthly distribution of precipitation through the years (Hovmöller plot). La Hilda for the period 2009-2020 and Fraijanes, for the period 1980-2020.*

3.2 Characterization of rainfall events

The distribution of the number of events for the available record at La Hilda (2009-2020) and per month is shown in Figure 3.2. Light rain dominated the rainfall events, with heavy and very heavy events occurring at a lower frequency and often associated with the occurrence of tropical cyclones. An example was hurricane Eta in November of 2020 (Table 3.1) for which daily accumulated rainfall reached almost 200 mm. Despite the dry season being less active, there were a few moderate rainfall events in the record. After the transitioning to the first leg of the rainy season in April, the number of moderate and rather heavy events increased and, between May and October there was a significant increase in moderate and rather heavy events. As expected between July and August a decrease was observed due to the influence of the MSD. For the 2009-2021 record, a total of 58 heavy precipitation events and 3 very heavy events were recorded during the rainy season. Higher intensity events occurred mainly from September to November, which were the months where our country is affected by tropical waves and hurricanes. The precipitation for very heavy rainfall ranges from 134 to 166 mm and for heavy rainfall ranges from 66 to 112 mm. It should be noted that the years that correspond to an ENSO event in the negative phase (La Niña) present a greater number of heavy events compared to the years in the positive phase (El Niño).

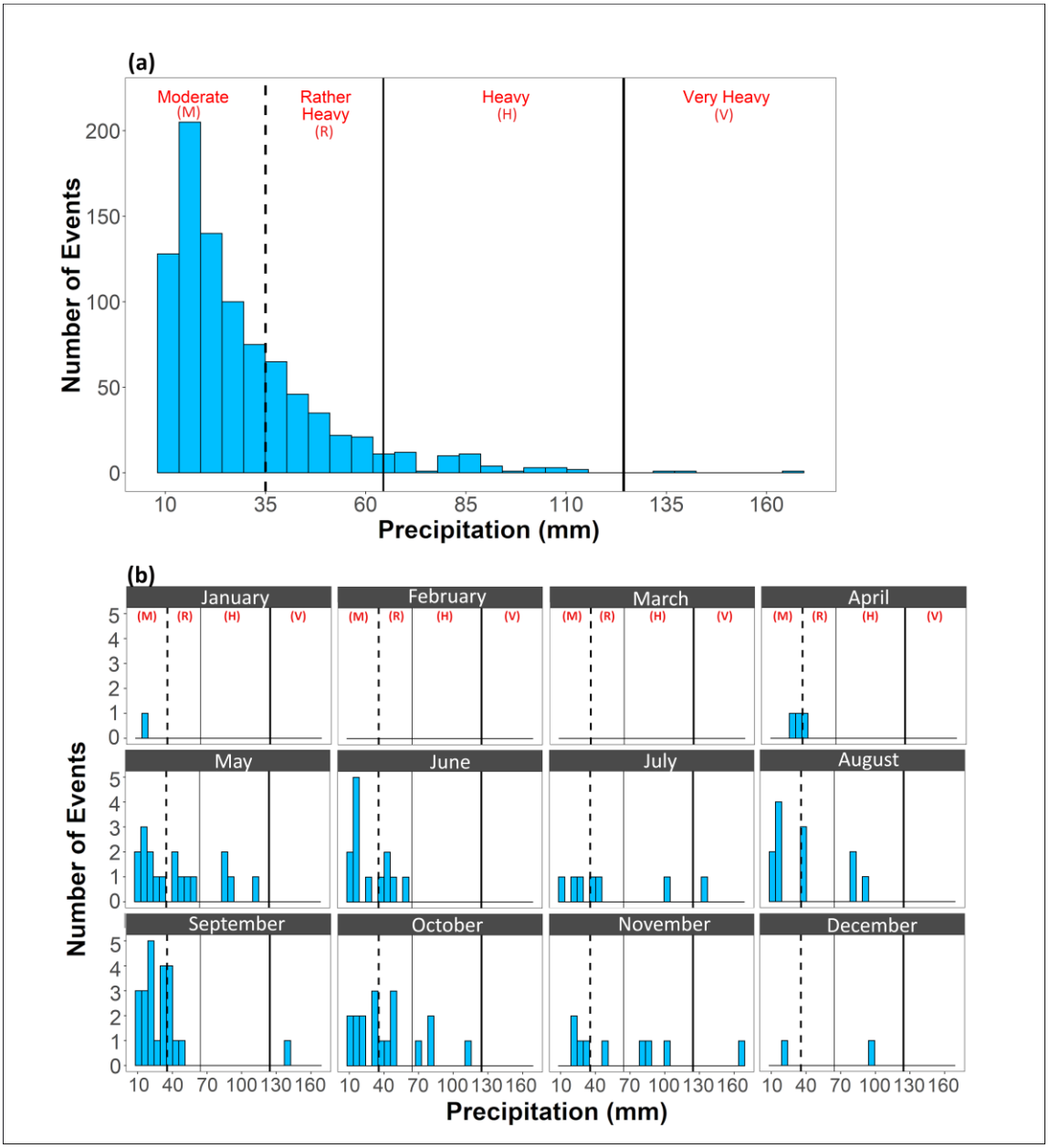

Figure 3.2 *(a) Distribution of the number of events at La Hilda according to the precipitation intensities from 2009-2020. (b) Distribution of the number of events per month for the year 2020. Plots (a) and (b) are separated from left to right as follows: moderate, rather heavy, heavy, and very heavy rain, based on table 2.1. 1000 days with precipitation in the light category between 2009-2020 and about 30 days for the months of the dry season in 2020 and a continuous decrease towards the rainy season.*

3.3 Heavy rainfall events (2020-2021)

The Events to be analyzed in terms of intensity were characterized by having an amount greater than 70 mm/day (Table 3.1) and, according to Table 2.2 are classified as heavy and very heavy rainfall events. The main modulators of heavy rainfall events were the ITCZ and the tropical waves. Previous studies (Durán-Quesada et al., 2017; Durán-Quesada et al., 2020) showed that the ITCZ and the cyclone activity are the main drivers for regional precipitation, particularly heavy rainfall events. Furthermore, heavy rainfall events are often associated with a poleward displacement of the ITCZ and to the weakened Caribbean trades (Hidalgo et al., 2019). As shown in Annex, the cloud cover maps for the selected events feature a high percentage of cloud cover and the positioning of the ITCZ over the country.

Date	Rainfall (mm/day)	Main systems associated with the occurrence of rainfall events
05/16/2020	87.4	ITCZ over Costa Rica, warming and entry of westerly winds and MJO.
05/21/2020	83.8	Tropical Wave. MJO and the ITCZ.
07/27/2020	134.4	Tropical Wave and instability due to the ITCZ.
08/04/2020	82	Cloud cover with a higher water vapor content in the atmosphere
08/05/2020	92.8	Close and active ITCZ, in addition a trough in height deepens to medium and low levels and warm morning temperatures
08/19/2020	81	Tropical wave and the ITCZ
10/15/2020	80.5	MJO, ITCZ and moderate trade winds.
10/16/2020	82.3	MJO, ITCZ and moderate trade winds.
10/30/2020	112.3	Tropical Wave and MJO.
11/01/2020	87.1	Hurricane Eta
11/03/2020	101.9	During the first week of November there were very humid conditions due to the indirect influence of hurricane Eta.

11/04/2020	166.1	During the first week of November there were very humid conditions due to the indirect influence of hurricane Eta.
11/05/2020	79.1	During the first week of November there were very humid conditions due to the indirect influence of hurricane Eta.
12/30/2020	95.5	Moisture ingress due to ITCZ and a low-pressure system forming in the eastern tropical Pacific
05/28/2021	70.6	Moisture ingress due to ITCZ
06/07/2021	109.9	Tropical waves and ITCZ
06/11/2021	80.5	Tropical wave and ITCZ
07/27/2021	107.4	Tropical waves and ITCZ
08/21/2021	101.6	Tropical waves and ITCZ
09/13/2021	89.4	Tropical waves and ITCZ
09/15/2021	111.2	Tropical waves and ITCZ
09/23/2021	107.7	ITCZ

Table 3.1 *Events with accumulated daily precipitation greater than 70 mm between 2020-2021, which corresponds to the categories rather heavy and very heavy (Table 2.1) and the rainfall producing system for each one. Likewise, the main event is the indirect influence of the Eta hurricane in November 2020.*

3.3.1 La Niña conditions during 2020-2021

ENSO plays an important role in the modulation of tropical cyclones activity (Ahrens & Henson, 2009; Duran-Quesada et al., 2020). During cold ENSO events (La Niña), the amount of heavy and very heavy events tends to increase at La Hilda. Such was the case for the analysis period, 23 strong events occurred, from which those with rainfall exceeding 75 mm/day were selected as threshold for the heavy rainfall events (Table 2.2). In August 2020, ENSO transitioned to La Niña, with its maximum intensity in October (-1.26) and November (-1.42) and ending in May 2021 (-0.46). This La Niña event in 2020, jointly with higher-than-normal sea surface temperatures in the tropical Atlantic affected the rainy season in Costa Rica due to the modulation of both the ITCZ activity and the tropical cyclone season.

The 2020 tropical cyclones season ended with a new historical record of tropical cyclones, accounting for a total of 30 events (13 hurricanes and 17 storms), surpassing the historical record for 2005 (28 events). During the 2020 tropical cyclone season, hurricane Eta was formed and it was highlighted to be the second most intense cyclone, causing severe impacts in Central America (IMN, 2021b; NOAA, 2020).

3.3.2 Eta Hurricane

Hurricane Eta reached category 4 on the Saffir Simpson scale; according to Pasch et al. (2021) it began as a tropical wave on October 22nd off the west coast of Africa. By October 31st the system's deep convection quickly became more organized over the east-central Caribbean Sea, with evidence of band structure formation. On November 1st at 0000 UTC, it strengthened and became a tropical depression, on November 2nd at 0600 UTC Eta turned into a hurricane at a speed of 36 m/s. Eta intensified rapidly and on November 2nd at 1800 UTC it reached category 4 at 59 m/s. The maximum intensity peak was observed on November 3rd at 0000 UTC with 67 m/s (Figure 3.3). Eta made landfall in Nicaragua on November 3rd around 2100 UTC as a category 4 hurricane. The abundant moisture associated with Eta and its remnants, together with the slow movement of the hurricane upon landfall, caused an extended period of heavy precipitation throughout Central America. On November 5th at 0000 UTC Eta became a tropical depression near Tegucigalpa, Honduras. The extreme rainfall associated with Eta caused catastrophic flash flooding, river flooding, and deadly landslides across the region.

According to the IMN, in the case of Costa Rica, the maximum recorded precipitation during the 5 days Eta's influence was 624 mm in Perez Zeledón, in San José province, the daily maximum was on November 5th with 226 mm. Figure 3.3 shows the evolution of Eta in the Atlantic for the days in which the daily accumulated rainfall exceeded 70 mm (heavy rainfall) at La Hilda between November 1st and 5th, the total accumulated rainfall over these 5 days was 455 mm. Maximum rainfall occurred on November 3rd and 4th with amounts that exceeded 100 mm/day, it is worth noticing that despite the influence of Eta over Costa Rica was classified as indirect the center of low pressure is very close to the country.

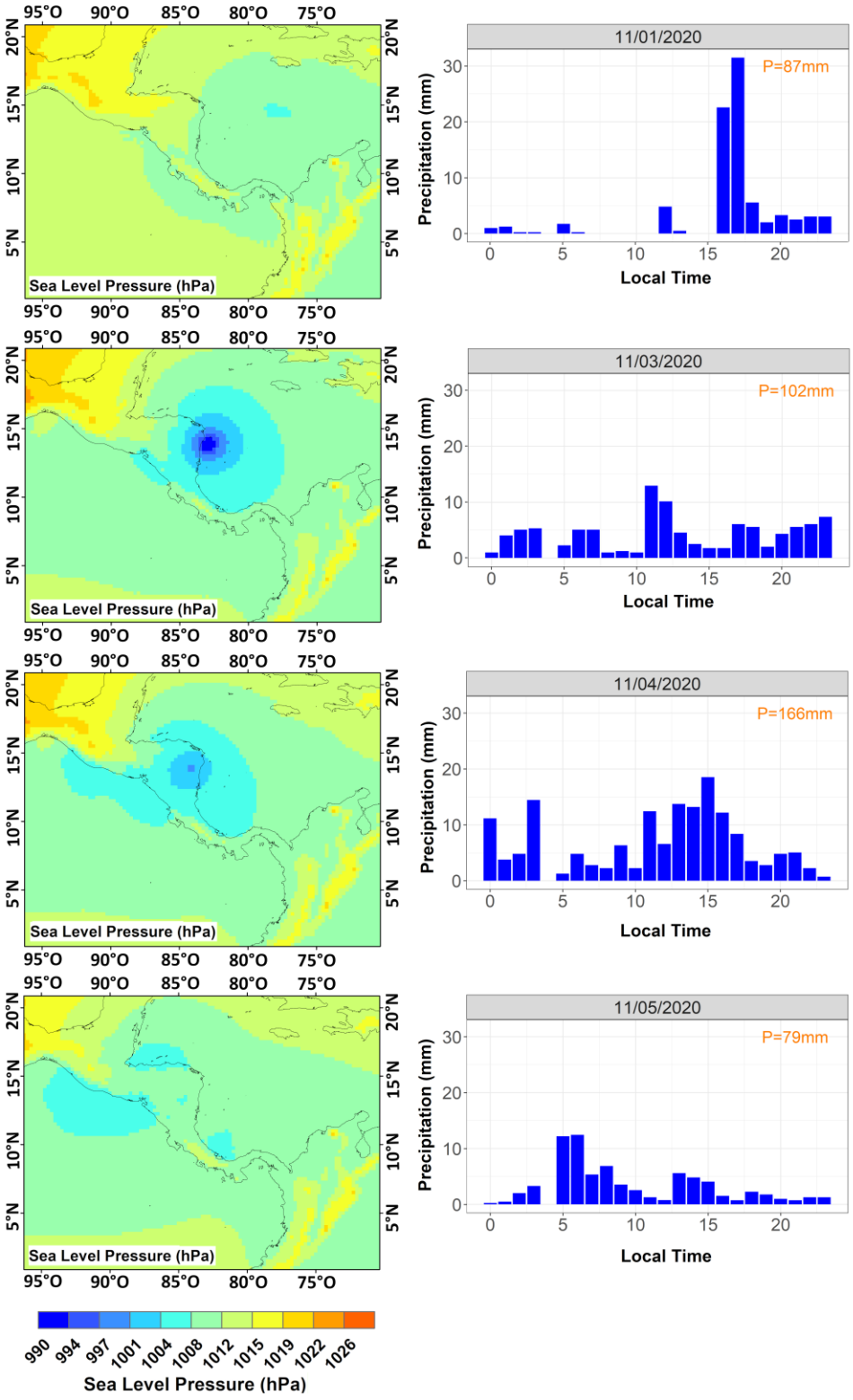

Figure 3.3 Left column: *Sea surface pressure (hPa) during the development of hurricane Eta, blue colors indicate the lowest pressure.* ***Right column:*** *Diurnal cycle of precipitation at La Hilda. In each graph the respective daily accumulation is observed in orange for days 1th, 3th, 4th and 5th November 2020.*

4. CO_2 and surface fluxes

4.1 Diurnal Cycle

The diurnal cycle is primarily controlled by the incoming solar radiation. In diurnal cycles for H, LE, and CO_2 fluxes negative values indicate downward flux (atmosphere to surface), and positive fluxes indicate upward flux (surface to atmosphere) (Figure 4.1). During the day, the net CO_2 flux is negative due to the photosynthesis process dominating over respiration, on the contrary, at night the net flux is positive. Overall, the total net flux is negative, associated to the larger assimilation of CO_2 during the photosynthesis process than a release of CO_2 through respiration. On another hand, H and LE fluxes have their higher values during the day and have their maximum between 10 am and 12 pm (local time) following the diurnal cycle of incoming solar radiation.

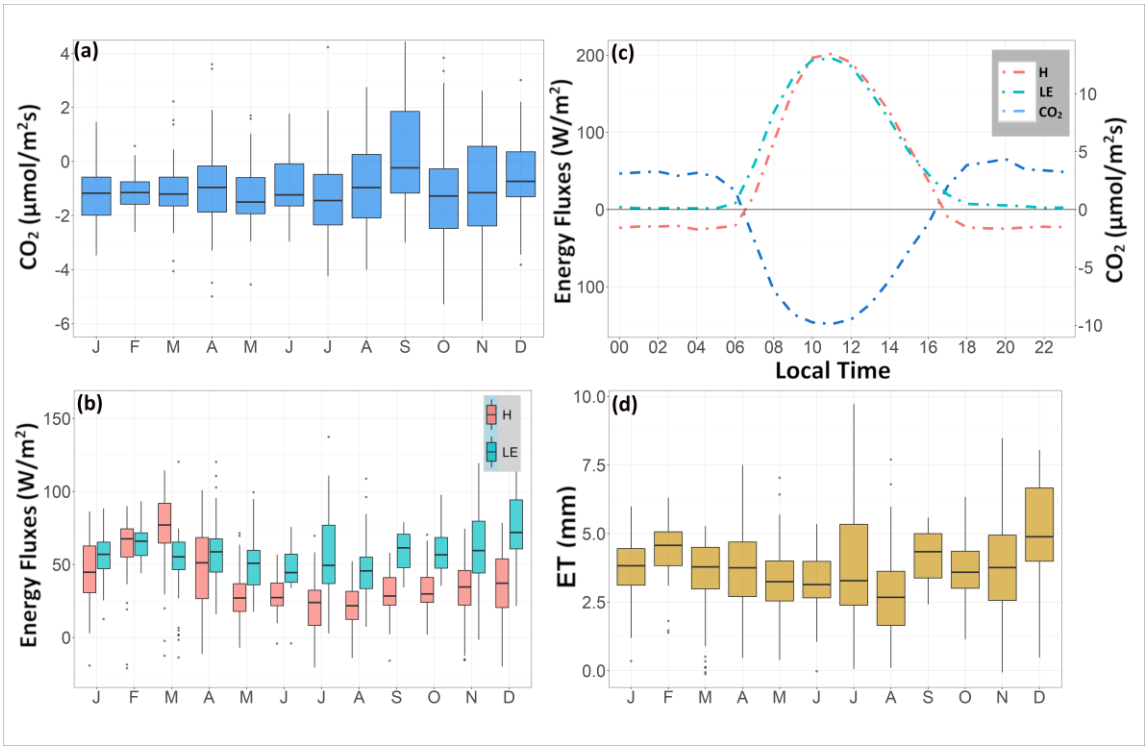

Figure 4.1 *Monthly distribution of the net CO_2, LE, H and ET fluxes for the period 2009 - 2021 for the full-sun EC tower at "La Hilda". (a) CO_2 flux (blue boxes) with ranges between -6 to 4 µmol/m²s with less variability in the months of the dry season. (b) LE Flux (green boxes) and H Flux (Orange boxes) with a range between -50 and 150 W/m². (c) Diurnal cycle of energy fluxes (H and LE) and CO_2 flux at La Hilda for 2020. (d) ET (yellow boxes) with values between 0 and 9 mm/day and less variability during the dry season.*

4.2 Annual Cycle

The energy and mass fluxes depend of the roughness of the surface, as a change in the vegetation cover could reduce or increase the turbulence in the boundary layer and as a result, the transport of energy and mass (Davin & de Noblet-Ducoudré, 2010). Because the surface fluxes are largely constrained by the vegetation, those fluxes have a very local character. In the case of the FS, the CO_2 flux was mostly negative (Figure 4.1c, blue line) which showed the dominance of atmospheric CO_2 uptake by the canopy. During the 2020-2021 period, the CO_2 was being mostly captured by the plants relative to the surface-atmosphere flux generated through respiration. The LE flux (Figure 4.1b, green box) can be understood by its relationship with ET (figure 3.2d), as, LE is the energy transferred to the atmosphere, due to, water transpired by plants and evaporated from leaves or soil surface (Lieth & Werger, 2012; Chapin III et al., 2011). At La Hilda, the values of LE range from 0 to 100 W/m^2 daily. The LE flux is also related with the H flux (Figure 4.1b, orange box), a decrease in ET can increase surface temperature and therefore H flux increases. In this case, like LE flux, H flux varies between 0 and 100 W/m^2 per day.

The fluxes had a marked annual cycle (Figure 4.1a, b and c). CO_2 showed less variability in the first leg of the rainy season and in the dry season. In the second leg of the rainy season (July to October) the CO_2 flux was more variable, which may be due to those months being characterized as the rainiest in this region (Figure 3.1). Likewise, LE exhibited a larger variability during the wetter months compared to the dry months, opposite to H that had a larger variability during the dry months, mainly in February and March. Variability of ET was higher during the second leg of the rainy season compared to the dry months. In addition, if the diurnal cycle per month was analyzed (not shown), LE had its maximum in October, while H had its maximum in March, and CO_2 had its down maximum flux in August. This behavior is explained by the relationship between the fluxes, the moisture availability and temperature, which affect the ET and hence the rate of photosynthesis (Bhatla & Lal, 2018).

4.3 Seasonal Cycle

The monthly distribution of fluxes for 2020-2021 was analyzed (Figure 4.2). In the case of LE (Figure 4.2a), during 2020 the largest day to day variability was observed for March, this variability was greater compared to 2021, however, it was observed that the means between these two years were similar. Despite April 2021 being rainier than 2020, LE flux was similar to 2020 with slightly higher variability and mean for 2021. It is important to mention that a year-to-year comparison for the first leg of the rainy season was hindered by missing data during both years for that period due to technical (power) issues with the monitoring system. During the second leg of the rainy season, the main difference between 2020 and 2021 was observed for July, the LE flux in 2021 was lower and in August it was slightly higher than 2020, which could be linked to differences in the MSD onset and duration. During the MSD, LE flux exhibited a larger variability during 2021. Likewise, it can be taken into account that although the difference in rainfall during the MSD between 2020 and 2021 was not significant (on average the accumulated rainfall was 0 mm) there was a difference in duration, since, for 2020 the MSD occurred in a period of 21 days (July 3th to July 24th) and for 2021 it lasted 11 days (July 10th to July 22nd)

H flux, unlike LE, was observed to be higher during the dry season in the two years (Figure 4.2b). There was a small difference in April, with a higher variability during 2021. In the second part of the rainy season, as with LE, the largest difference was observed between the third part of July and August. It is interesting to emphasize that although changes in ET (LE flux) influence the ambient temperature (H flux) (Davin & de Noblet-Ducourdré, 2010; Perugini et al., 2017), it was not observed that changes in LE directly affect H, that is, the values of LE during the year remain very similar (average between 40-80 W/m^2), however, H did have a marked difference between the dry and rainy seasons.

The CO_2 flux during the dry season (Figure 4.2c), the average daily values tend to zero and were similar for the two years, with slightly larger variability during March and April for 2020. During the MSD, the variability was larger for, during 2020 the net flux was negative but tended to zero in 2021. It should be noticed that the difference in the fluxes

during the MSD for 2020 and 2021 may be because during 2020 the MSD had a longer duration, it lasted approximately one more week compared to 2021. During the second leg of the rainy season, it was observed that during 2021, mainly in the months of August to December, the CO_2 flux presents a larger variability and a higher tendency towards positive values than in 2020. In 2020, the values mostly tended to a downward flux and present less variability in the month of September.

In the case of rainfall (Figure 4.2d), during the dry season both 2020 and 2021 the mean rainfall was 0 mm, and the most important difference occurred during the transition to the first leg of the rainy season in April 2021, which featured a larger rainfall variability. During the first leg of the rainy season, the largest difference was observed in May and the first part of July. In May 2020 there was a higher variability of precipitation and on average it rained more than in 2021, likewise, the first week of July presented more precipitation in 2021 than in 2021 with a difference in the means of approximately 50 mm. The MSD period for both 2020 and 2021 had low rainfall, with a mean of approximately 0 mm. Finally, in the second part of the rainy season, the largest difference between these two years was in the third part of July and October. However, August and September also differ in the mean values and variability. More specifically, August and September 2021 show higher variability. The month of October 2021 was characterized by a deficit in precipitation at national level. November 2020 had more variability than 2021, but the means were similar. For both 2020 and 2021 a drop in the SWC was observed during the dry season, which changes with the beginning of the rainy season, where there is a notable difference, with an increase in SWC. However, this increase remains stable throughout the rainy season (Figure 4.2e).

On the other hand, the variations during the establishment of the MSD were slight, with a small decrease in the SWC. In general, the months that presented the greatest differences between one year and another are February with a higher SWC for 2020, the first part of July, November and December with a higher value for 2021.

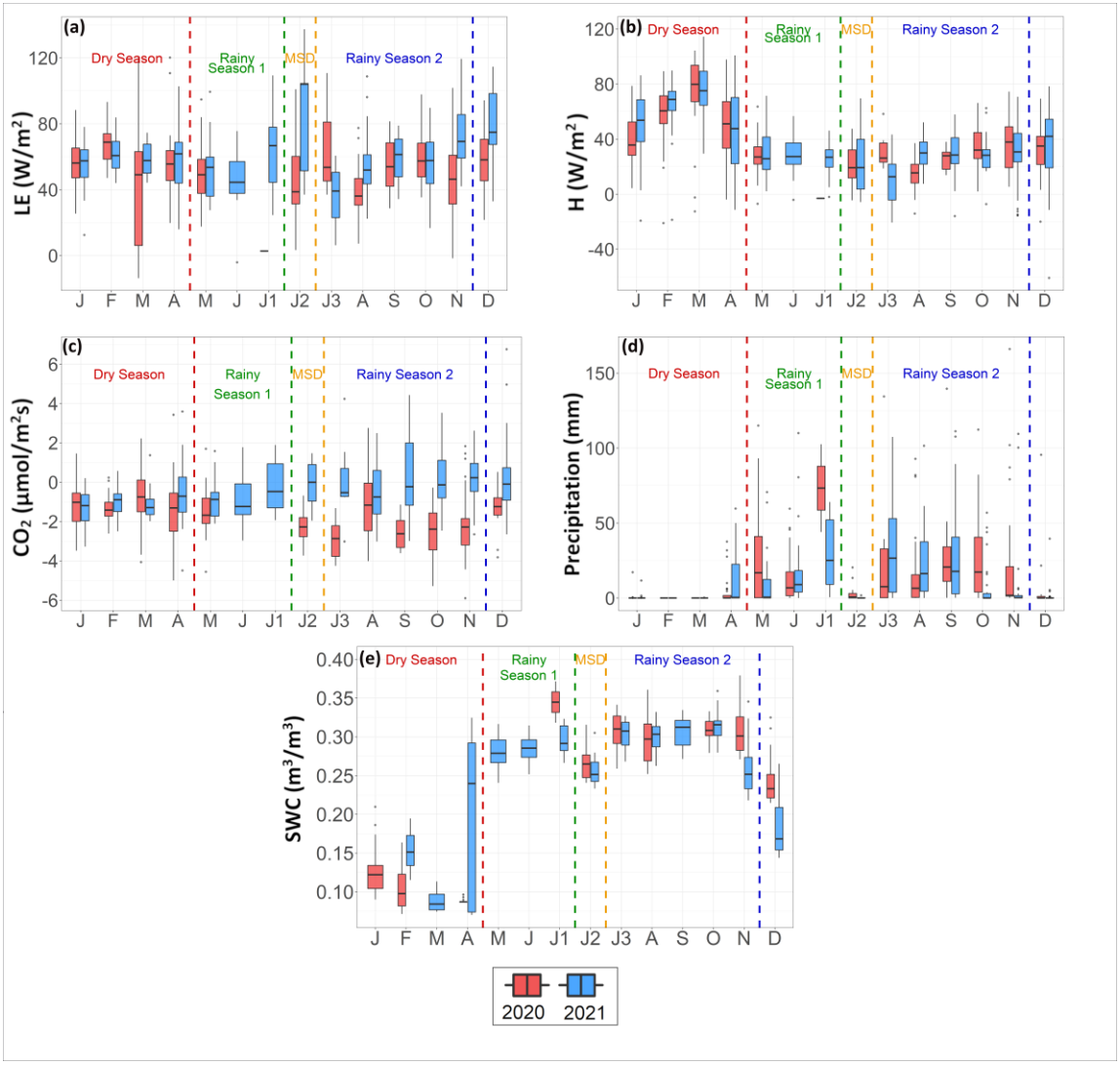

Figure 4.2 *Monthly distribution of energy fluxes, CO_2 flux and SWC for 2020 and 2021 (red and blue boxes, respectively). The different dotted lines separate the boxplot according to the seasons of the year, dry season, rainy season 1, MSD and rainy season 2, respectively. The values J1, J2 and J3 correspond to the month of July, where J2 are the days that correspond to the MSD, July 3th to July 24th 2020 and July 12th to July 22th 2021.*

4.4 Discussion

The CO_2 flux varies during the year and it responds to variations in rainfall amount and intensity (Mölders & Kramm, 2014). CO_2 flux had greater variability in the second part of the rainy season (Figure 4.1a), this part of the year was characterized by being the rainiest and, furthermore, it was in this second part of the rainy season where the cases of moderate rather heavy rain increase (Figure 5.1).

The diurnal cycle of LE flux is related with the diurnal cycle of ET of the crop (Lieth & Werger,2012), and depends on the soil moisture since a lower soil moisture content translates into stomatal closure due to water stress and, therefore, reduces plant transpiration (Figure 4.1c, Fahad et al. 2017). Hence, the diurnal cycle of LE was related to the diurnal cycle of CO_2 because plants take more CO_2 during the photosynthesis and at the same time lose water through transpiration, which is why a maximum of LE was observed at the same time that the maximum uptake of CO_2 occurs (higher negative values). Stomatic transpiration is the mechanism that drives the loss of water. However, this can be affected by different factors, including environmental factors that can lead to stomatic closure such as the increase in temperature that causes an increase in the transpiration rate, up to a certain threshold (Bhatla & Lal, 2018). The maximum diurnal heating occurs between 10 am and 12 pm, hence a larger ET would be expected, which was reflected in the maximum LE as a response to the diurnal heating. The decrease in LE during the afternoon is related to condensation cooling, which in many cases brings with it the afternoon rains (Lieth & Werger,2012) and the maximum of H occurs between these hours due to the increase in temperature. As LE is strongly linked to ET, which varies according to the availability of soil water; on the other hand, H is a measure of the variation of the ambient temperature (Lieth & Werger,2012).

The intraseasonal variability of these fluxes is influenced by variables such as cloudiness, rain, and temperature, because cloudiness has an important effect on the daily temperature range. Monthly precipitation influences soil temperature and moisture; therefore, the daily variation of weather influences the monthly variability of H and LE fluxes.

4.4.1 Intraseasonal variations

As shown in section **4.3 Seasonal Cycle** , the main differences between 2020 and 2021 occur for CO_2 and LE fluxes. Those differences in the fluxes were associated with the behavior of precipitation for 2020 and 2021, as 2021 was featured by an anomalous October, with a deficit of precipitation at the national level (Figure 4.2d) and the establishment and duration of the MSD varied from one year to another. During the

establishment of the MSD in 2021, the higher flux of LE translates into a higher ET (approximately 67 mm) that decreased in the third week of July (Figure 4.2a, J3). The latter contrasted with a lower ET (approximately 63mm) during the MSD for 2020. In late July 2021 a storm that significantly affected the North and Caribbean regions of Costa Rica developed; although it did not directly influence La Hilda, it affected the distribution of moisture and increased cloudiness, which seems to have effected CO_2, LE and H. In addition, the fact that H was higher during the dry season could be linked to what was mentioned by Bonan (2005) regarding the fact that if the soil is dry, the net radiation on the surface is converted mainly into H. During the second leg of the rainy season of 2021, there was a tendency of positive CO_2 flux that likely corresponded to a higher respiration rate. Despite the positive CO_2 flux was larger in September and October, the trend of higher respiration rates started during the MSD. Soil temperature and soil moisture (soil water content, SWC) are the most important environmental factors affecting soil respiration (RS, including respiration by plant roots and soil microorganisms), SWC is responsible of 70% of RS variability, soil temperature of 25% and vegetation cover of 3%, approximately (Arredondo et al., 2018).

5. Response of surface fluxes to heavy rainfall events

5.1 Impact of heavy rainfall on surface fluxes

Weak, moderate, and rather heavy rainfall events were mainly associated with the ITCZ, while heavy and very heavy rainfall events occurred mostly due to the development of tropical waves and the indirect influence of a hurricane. Rainfall at *La Hilda* is variable throughout the year and the seasonal distribution of precipitation is reflected in the variability of the surface and energy fluxes. The variability of CO_2 flux was different comparing light and moderate events with the heavy rainfall events (Figure 5.1 left column). After mid-day, the variability of CO_2 for events of higher intensity was considerably reduced (especially with very heavy rainfall); in general, the CO_2 flux tends to zero as the amount of rainfall increases. The LE and ET fluxes variability (Figure 5.1 middle and right column) was also influenced by the intensity of precipitation. In all cases the variability of LE and ET fluxes decreased after noon, where the maximum intensity of precipitation generally occurs. This behavior was more noticeable when the rainfall was heavy, rather heavy, and very heavy. Maximum LE most frequently occurs at 10:00 (but ranges from 10 am to noon) and the maximum rainfall mainly occurs at 15:00 (but ranges from 02:00 to 23:00).

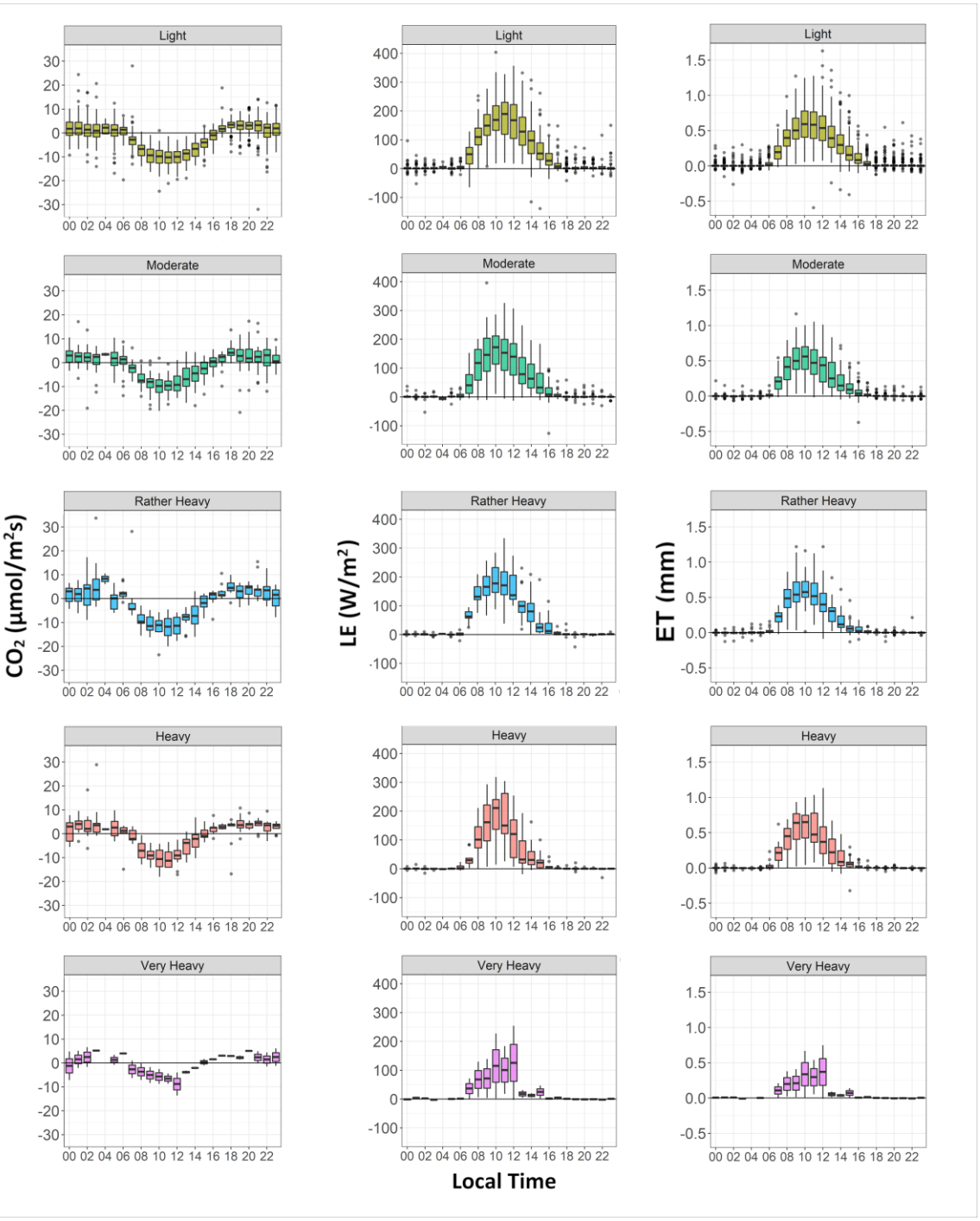

***Figure 5.1 Left column**: Diurnal cycle of CO_2 for each rainfall category for 2020-2021. Each panel shows how the variability changes through the different categories of precipitation. **Middle column:** Diurnal cycle of LE for each rainfall category. **Right column:** Diurnal cycle of ET for each rainfall category. At La Hilda for the period 2020-2021 for each category of precipitation (Table 2.2).*

The behavior of the fluxes of CO_2, H and LE was significantly influenced by heavy and very heavy rainfall events of precipitation (Table 2.2, Figures 5.2, 5.3 and 5.4). CO_2 flux maximum fixation occurred between 9:00 and 15:00 hours (Figure 5.2). The CO_2 flux responses to the events varies depending on the duration of the event. When precipitation events last all day (Figure 5.2g and h), CO_2 fixation was lower compared to short-duration events where the precipitation had a maximum at specific hours, that is, it has a marked diurnal cycle. It must be pointed out that for the analysis period the long-duration events were associated with the influence of hurricane Eta, which albeit lasting for 5 days had major impact on the site during the last three days of its life cycle. Also, for short-duration events, the maximum atmosphere to surface flux (negative) generally occurs before the maximum precipitation peak.

The monthly diurnal cycle was compared with the diurnal cycle of each event for CO_2 and LE (Figures 5.2 and 5.3). It can be noticed the behavior of the fluxes changes between the events and are modulated by the monthly cycle. For short-duration events (Figure 5.2a, to 5.2f) the response of the CO_2 flux was similar to the monthly mean, however, for long-duration events, the negative CO_2 flux decreased with respect to the monthly values (figure 3.6g and h, values of 102, 106 and 79 mm). In the case of LE (Figure 5.3) the maximum of the events exceeded the monthly mean, which was expected since these are events that stand out compared to the average. For short duration events, the maximum LE values occurred approximately 4 hours before precipitation peaks. For long-duration events (Figure 5.3g and h, values of 102, 106 and 79 mm) LE was steady during the day, the behavior of CO_2 was similar as differences were hardly noticeable compared to the monthly diurnal cycle. The latter could be related to the number of precipitating days due to the influence of Eta hurricane. The H flux (Figure 5.4) showed higher variability for events of longer duration than for shorter ones. For events of shorter duration, the maximum of H occurs between 9:00 and 15:00 with daytime warming. It can be noticed that the variability of H does not only depends on the amount of rainfall but also on the way it is distributed throughout the day.

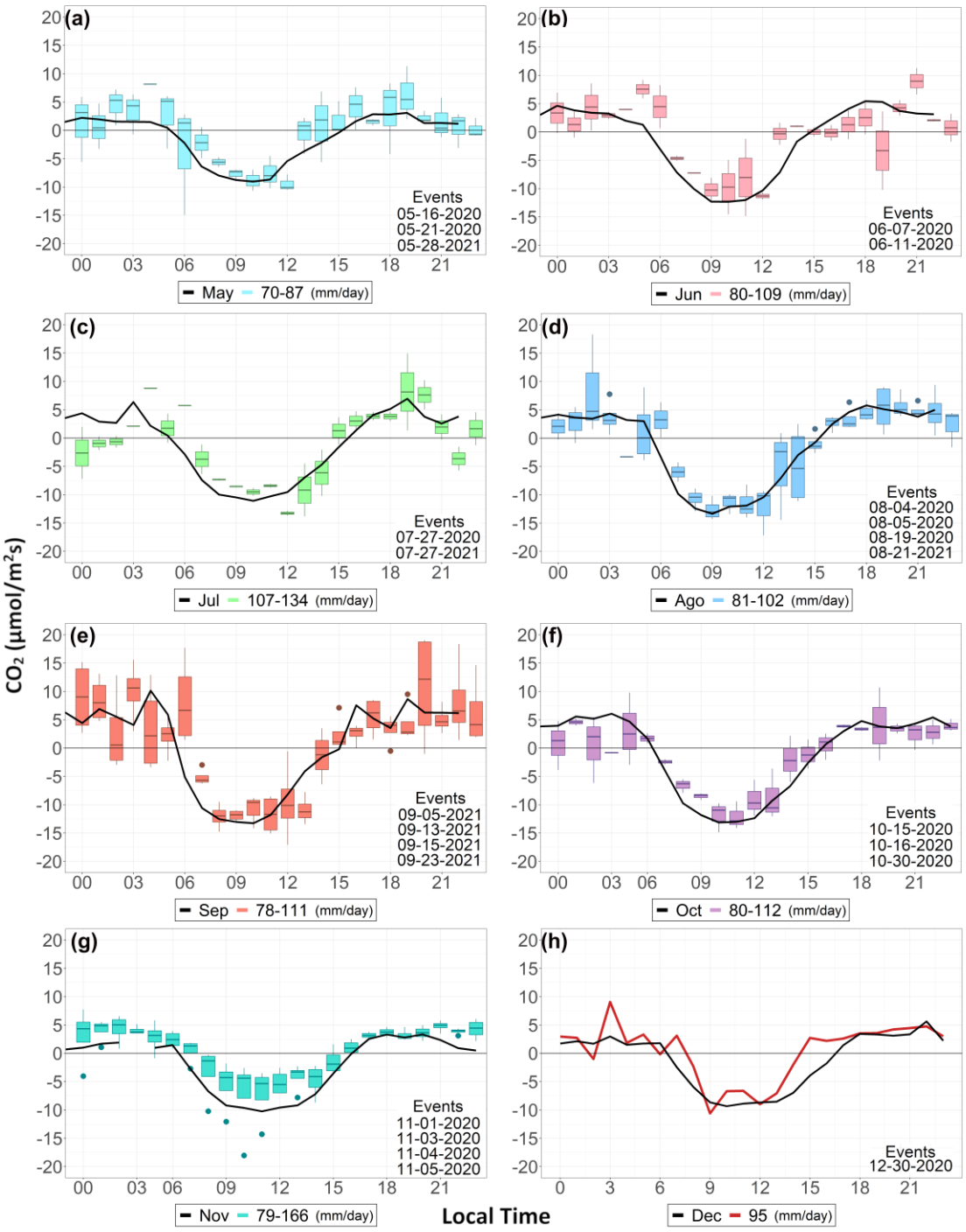

Figure 5.2 *CO_2 flux for the different events of precipitation compared with the diurnal cycle per month. Black lines represent the diurnal cycle per month during 2020-2021, and the boxplot represents the events listed in table 2.2. It is possible to observe that the behavior of the CO_2 flux depends on the amount of rainfall but also on the way it is distributed throughout the day.*

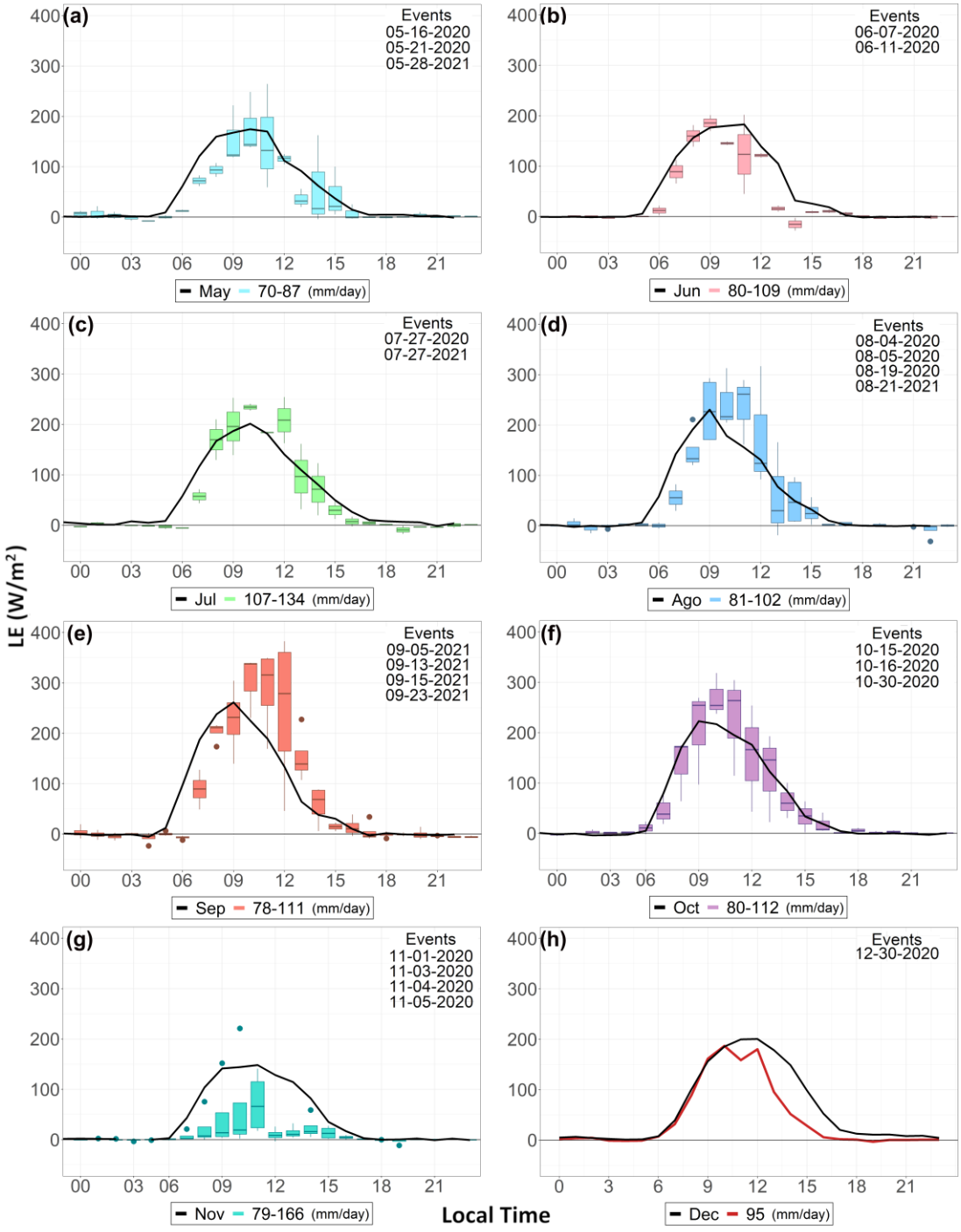

Figure 5.3 *LE flux for the different events of precipitation compared with the diurnal cycle per month**.** Line black represents the diurnal cycle per month 2020-2021, and the boxplot represents the events listed in table 3.2. It is possible to observe that the behavior of the LE flux depends on the amount of rainfall but also on the way it is distributed throughout the day.*

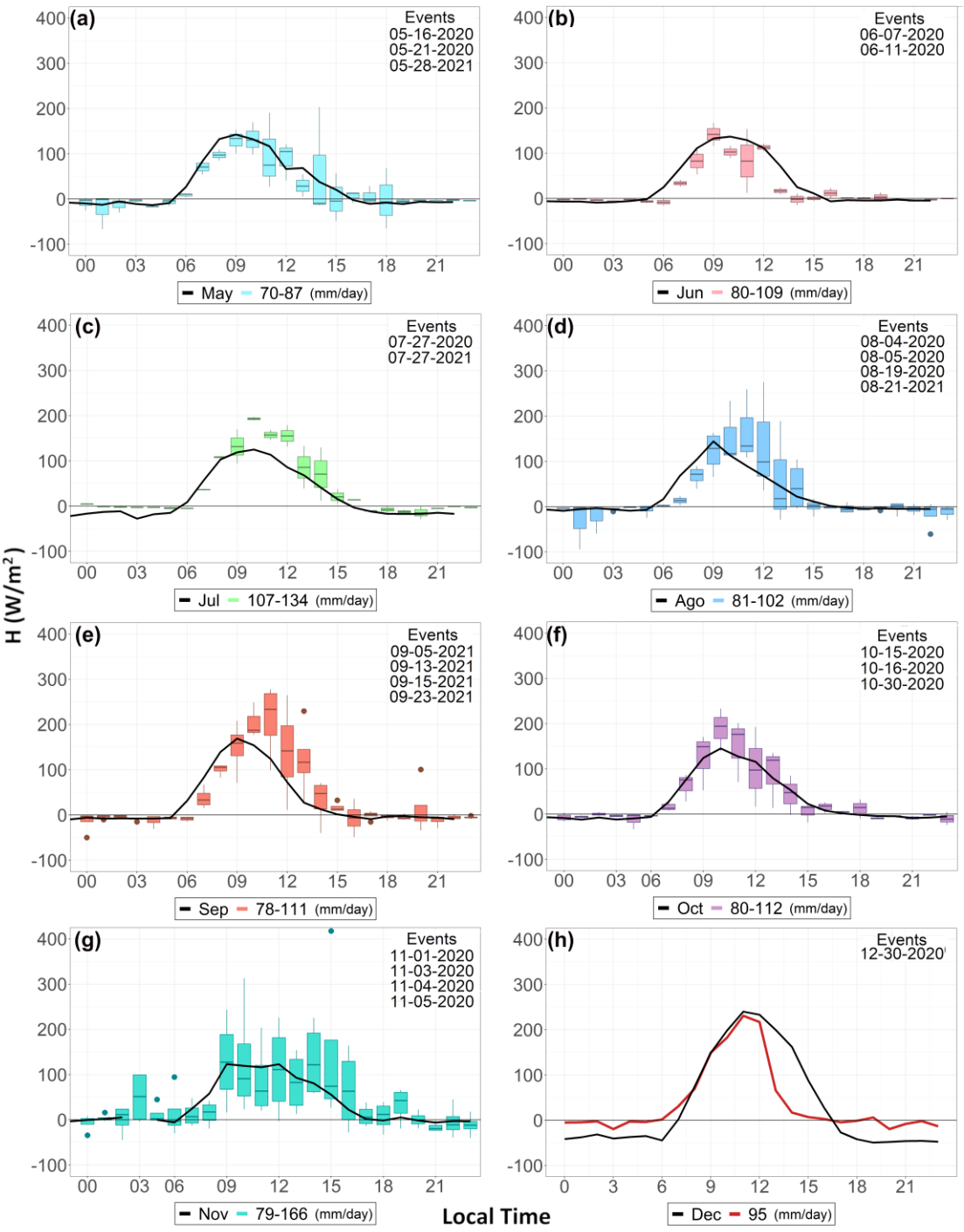

Figure 5.4 *H flux for the different events of precipitation compared with the diurnal cycle per month. Line black represents the diurnal cycle per month 2020-2021, and the boxplot represents the events listed in table 2.2. It is possible to observe that the behavior of the H flux depends on the amount of rainfall but also on the way it is distributed throughout the day.*

5.2 Discussion

The diurnal cycle of the surface and energy fluxes was influenced by the precipitation. Wu et al. (2003) showed that precipitation variability can affect GPP and Xiao et al. (2013) and Lal (2004) mentioned that LE flux has a strong linkage with the main components of the water cycle (precipitation, ET, and runoff) because it represents the ET, so water and energy balance are closely linked. The analysis of the fluxes for the different categories of precipitation (Figure 5.1) and by selected events, showed that the response of the flux depended on the amount of precipitation and the duration of the event (Figure 5.2 to Figure 5.4). In the diurnal cycle (Figure 3.8), the relationship between the diurnal heating leading to a maximum in the LE flux due to the increase in ET, and the maximum peak of precipitation after the maximum in this flux. This occurred because LE flux was related to the condensation potential which leads to the development of precipitation, in this case, especially in the afternoon. For long-duration events and very heavy precipitation (e.g hurricane Eta influence, Figure 5.3g and h) LE was almost constant during the day similar to CO_2 (Figure 5.2g and h). The latter in agreement with Chen et al. (2013) findings that state that under saturation of soil and vegetation due to abundant precipitation, vegetation ET and primary production (CO_2 flux) remain relatively constant.

Furthermore, cloud cover can influence the rate of photosynthesis and ET because when the cloud cover is dense during rainy conditions and low levels of photosynthetically active radiation (PAR) limit plant photosynthesis (Bermingham et al., 2005). PAR was not considered for this stage of the study, but it is suggested to further evaluate the impact of cloudiness on PAR and its role as a limiting variable for ET and photosynthesis in the FS. For the H flux (Figure 5.4), based on Wei et al. (2014) H is generated and transferred between the land surface and the atmosphere at a rate that varies with temperature. During heavy rainfall, this transfer can be large which can affect the local surface temperature on an hourly to daily timescale. In the case of the tropics the H could have a notable effect on the local surface temperature during a heavy rainfall event because the cooling effect is dominant due to the abundant rainfall and generally negative temperature differences between the land surface and rainwater. Therefore, this change in temperature between surface and rainfall could be responsible for the variability of H.

6. Soil analysis, water use efficiency and sap flux for heavy rainfall events 2020-2021

6.1 Soil analysis

The behavior of the SWC for heavy rainfall events at La Hilda was analyzed in comparison with the precipitation for each extreme event (Figures Figure 6.1 and Figure 6.2). In the case of rain, it can be seen that for short duration events, the SWC was constant during the day (always greater than zero) and increased with the onset of precipitation, that is, a change in the SWC was observed only when there was a marked diurnal cycle of rainfall. Authors such as Arredondo et al. (2018) and Jia et al. (2016), have investigated the SWC-Precipitation relationship, the former mention that SWC is a variable dependent on precipitation, however, the water holding capacity of the type of soil in the upper soil layer plays an important role in the SWC. Likewise, the latter mention that the characteristics of the rainfall (quantity, frequency and intensity) can affect both temporally and spatially the SWC. In fact, in their research they found that as rainfall increases (this for heavy rain events), the depth of water in the soil increases and with it the SWC increases.

Similarly, Jia et al. (2016) emphasize that the SWC was not only affected by the amount of precipitation, but also its intensity and frequency. On the other hand, in the case of the long-term event (Hurricane Eta, November 2020), since there is precipitation throughout the day, the SWC was nearly constant because in a saturated soil, the fluxes become almost constant (Chen et al, 2013). The behavior of the SWC with the diurnal cycle of the ET was a little different compared to that of the precipitation (Annex 2), since, in the maximum peaks of ET, which occur during the hours of maximum radiation, it was observed that the SWC was held constant, meaning an increase in ET did not influence the SWC loss or gain.

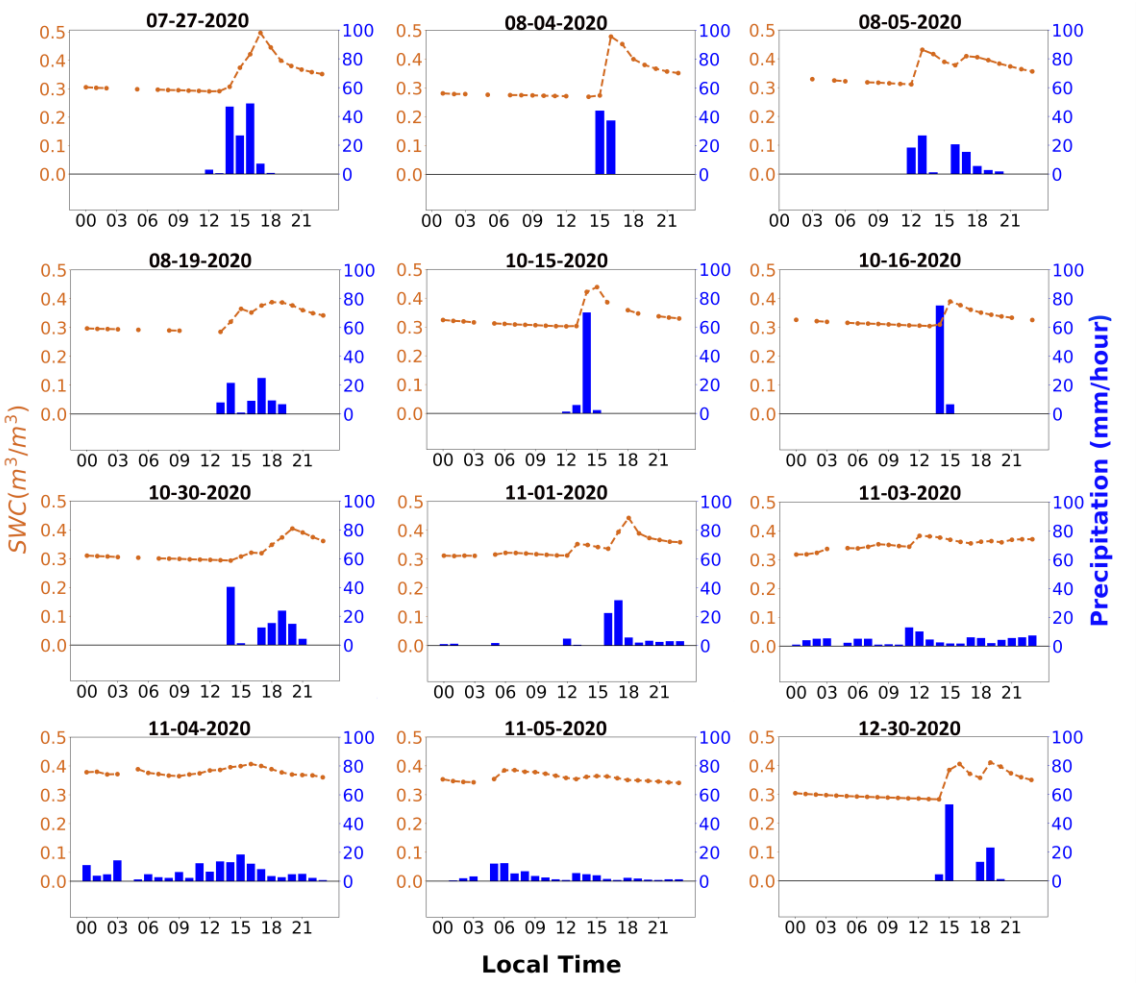

Figure 6.1 *SWC diurnal cycle (orange line) and precipitation (blue bars) for extreme rainfall events for 2020 at La Hilda (Table 2.3). November 2020 event is Hurricane Eta for which a different behavior of the SWC is observed with respect to rainfall compared to the other events.*

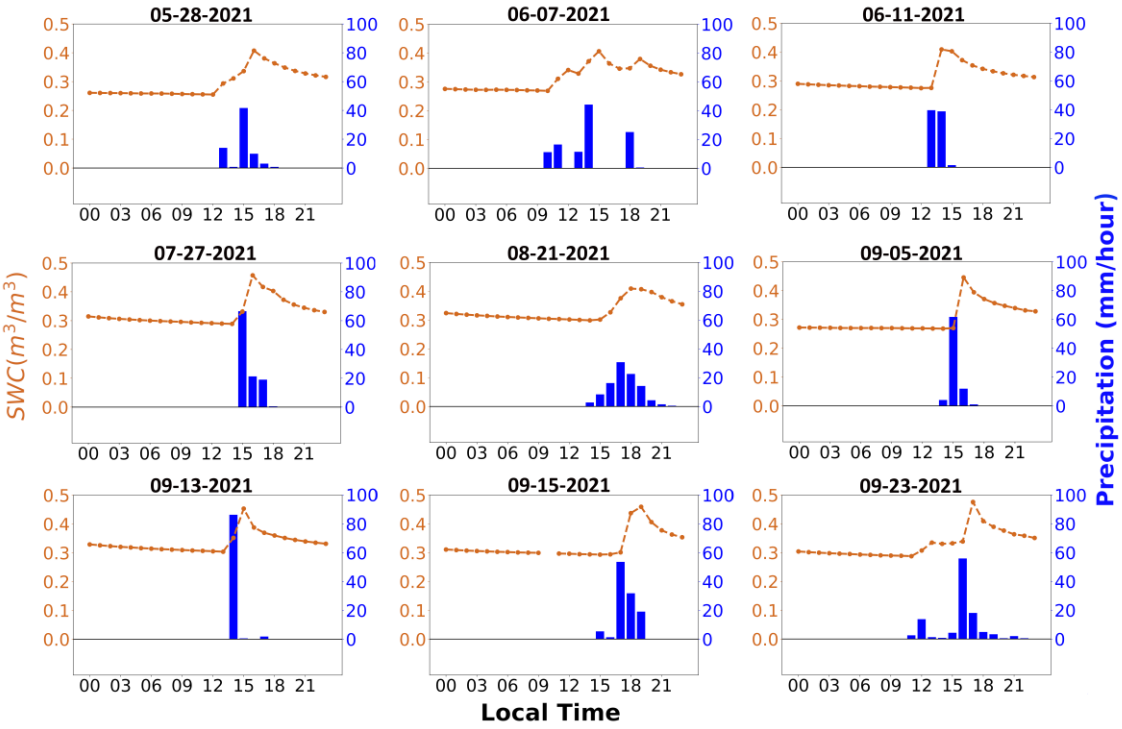

Figure 6.2 *SWC diurnal cycle (orange line) and precipitation (blue bars) for extreme rainfall events for 2021 at La Hilda (Table 2.3).*

6.2 Water use efficiency

WUE is related to the GPP, which is modulated by water, carbon and energy feedback between the canopy and the atmosphere (Chinchilla et al., 2021). WUE of the coffee plantation for 2020-2021 had the largest values during the second leg of the rainy season, that is, in the rainiest months (Figure 6.3). The main differences for WUE were observed for January, March, July, and November. January 2021 WUE was negative but almost zero, and in March and November 2020 WUE was larger compared to 2021. Meanwhile for July, WUE for 2021 was higher compared to 2020. The values of the WUE for the events of heavy and very heavy rainfall (Table 3.1) can be observed on Table 6.1. Highest values of WUE during heavy rainfall events occurred during the period in which La Hilda was affected by the indirect effect of hurricane Eta.

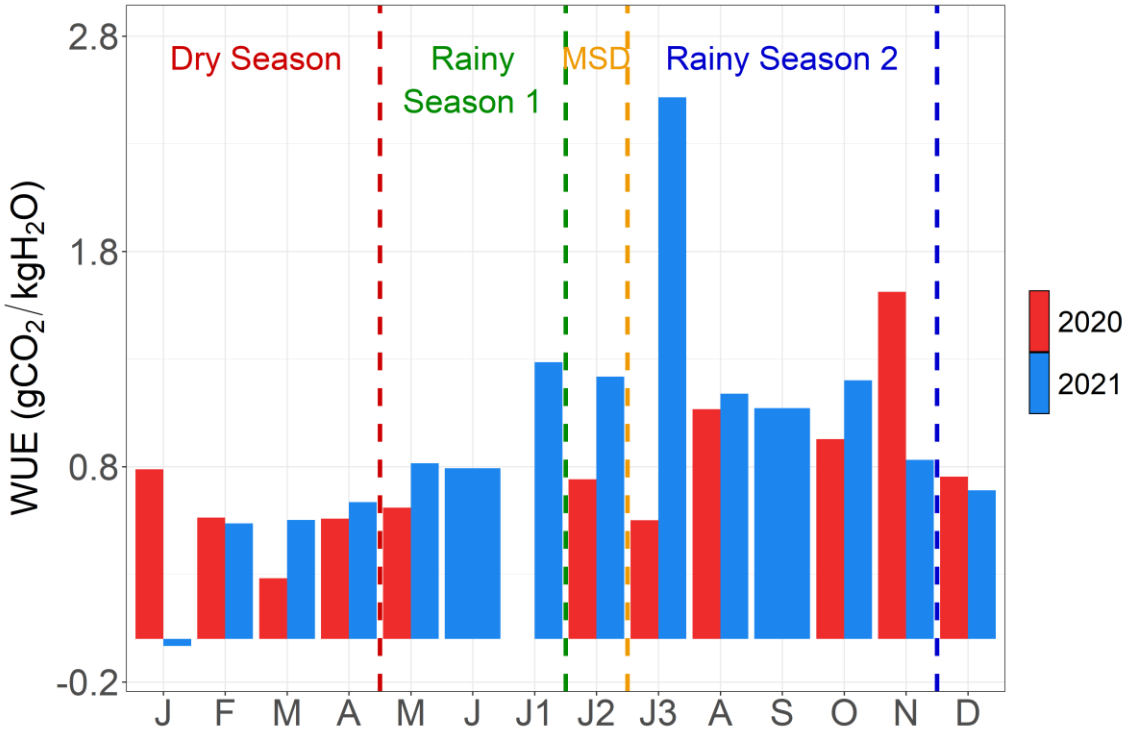

Figure 6.3 *Annual cycle of monthly averages of WUE (gCO_2/kgH_2O) at La Hilda, for 2020 in red and 2021 in blue. The largest WUE is observed in the second part of the rainy season which is the rainiest in this region. For 2020 there is no data in June and September. The values J1, J2 and J3 correspond to the month of July, where J2 are the days that correspond to the MSD, July 3th to July 24th 2020 and July 12th to July 22th 2021.*

Date	WUE	Date	WUE
16/05/2020	0.36	**04/11/2020**	8.67
21/05/2020	0.83	**05/11/2020**	2.86
27/07/2020	0.58	**30/12/2020**	0.62
04/08/2020	0.61	**28/05/2021**	1.13
05/08/2020	0.76	**07/06/2021**	0.57
19/08/2020	0.48	**11/06/2021**	1.36
15/10/2020	0.72	**27/07/2021**	0.77
16/10/2020	0.52	**21/08/2021**	0.90
30/10/2020	0.88	**13/09/2021**	0.57
01/11/2020	1.62	**15/09/2021**	1.03
03/11/2020	5.28	**23/09/2021**	1.02

Table 6.1 *WUE estimated for the events of table 2.2. The higher values of WUE (gCO_2/kgH_2O) can be observed during the dates that correspond to the effect of the hurricane Eta in November 2020.*

The WUE evaluates the capacity of the plants, depending on their specie, to gain or lose CO_2 and water, it is used to determine the efficiency of the plants to fix CO_2, relative to the amount of water loss by transpiration (Baldocchi. 1994; Bhatla & Lal, 2018). According to Xiao et al. (2013), annual WUE is related to annual precipitation and WUE increases as function of the ecosystem productivity. As shown in Figure 6.3, the intra-seasonal variability of the WUE is influenced by heavy rainfall events, for which the surface fluxes present the largest variations, the wettest months have higher WUE compared to drier months. WUE differences between 2020 and 2021 for March and July are a result of the differences in the surface fluxes for those months (Figure 4.2) as there is a marked difference in the variability between 2020-2021 for CO_2 and LE fluxes.

Similar was the case for July as differences in the onset and duration of the MSD induce differences in WUE during 2020 and 2021. In the case of November, in addition to having a difference in the fluxes, there was a difference in the variability of precipitation between these two years (Figure 4.2). The behavior of the WUE for the events in Table 6.1 and Figure 6.3 was related to the amount of precipitation, in agreement with findings that suggest that the increase in precipitation stimulates an increase in the WUE; on the contrary, dry conditions can cause a decrease in the WUE (Gu et al., 2021).

The most relevant event in this research has been the indirect influence of Hurricane Eta, in which marked differences have been seen in the response of the fluxes compared to other extreme events. In the case of the WUE, very high values were observed on the days when the hurricane affected, especially on November 3^{th} and 4^{th} of 2020 (Table 6.1). These high values can be related to the behavior of the ET and the GPP due to the abundant amount of rain. As mentioned above, ET was affected during Eta, exemplified by low values and an almost constant diurnal cycle (Figure 5.1). On the other hand, the GPP for this event presented low values compared to the other events, with differences of up to 100 gCO_2/m^2day. Authors such as Xiao et al. (2010) and Yuan et al. (2021) have investigated the relationship of the GPP with extreme events, and they have mentioned that the GPP is reduced at regional scales due to droughts, fires and hurricanes, in addition, it exhibits a strong spatial and seasonal variability which is due to the effects of storms,

climatic conditions and distribution of vegetation. Likewise, it is emphasized that in the tropics the GPP is more sensitive to changes in precipitation compared to temperature.

6.3 Sap Flux

Sap flux can be used as an indicator of plant water status, it measures transpiration as the ascent of sap in the xylem tissue (Gimenez, 2005; Chinchilla et al., 2021). Transpiration responds quickly to environmental changes in moisture and temperature; hence it is expected that sap flux would respond in terms of the intensity of the rainfall events. The behavior of the sap flow based on different rainfall intensities was analyzed (Figure 6.4, Table 2.2). It was noticed that while sap flux changes as the intensity of the precipitation increased, the main difference was more marked for heavier rainfall events (heavy and very heavy). In the case of heavy rainfall, it was observed how the sap flux was more uniformly distributed and it seemed that the data begin to concentrate mainly between 0-50 g/h and 100-200 g/h. Likewise, in the case of very heavy rainfall, the peak of the distribution was displaced to the right, showing a marked contrast compared to other rainfall intensities.

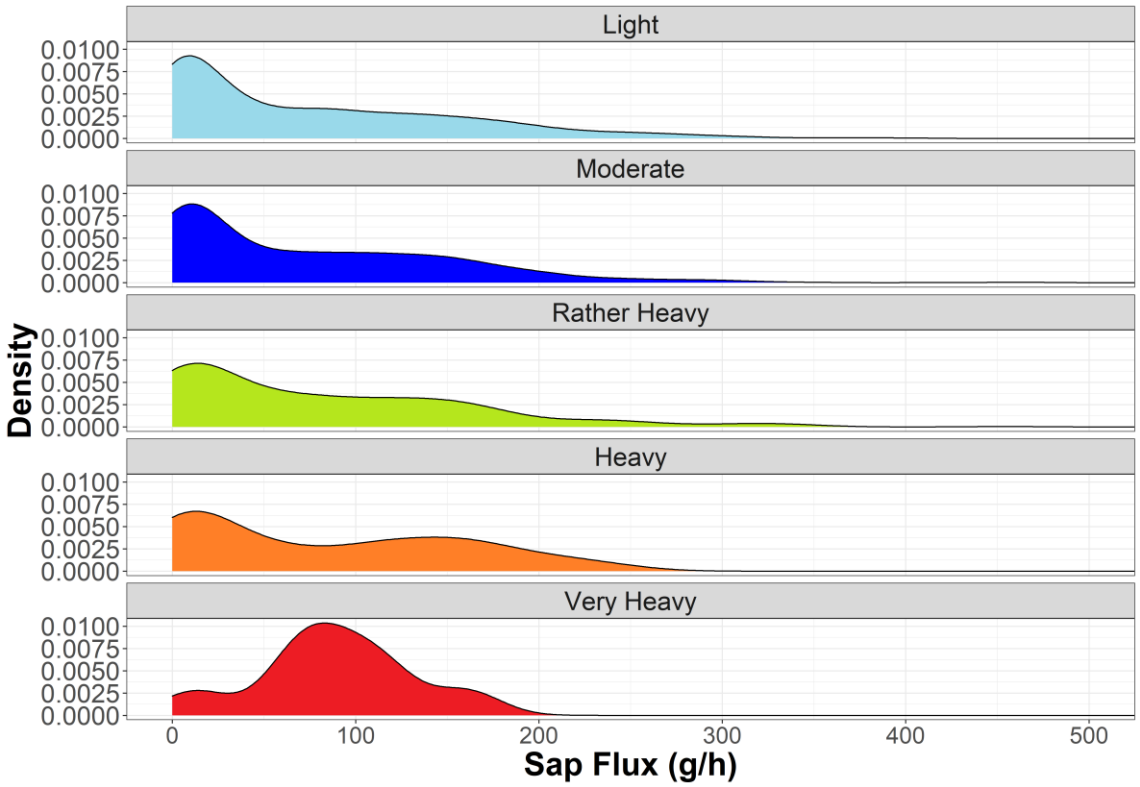

Figure 6.4 *Graph of the probability density function for the hourly flow of sap divided according to the different categories of precipitation in light, moderate, rather heavy, heavy and very heavy (Table 2.2)*

7. Conclusions and Recommendations

CO_2 flux showed greater variability in the second part of the year, specifically, the second part of the rainy season, where moderate to very strong rainfall events increased. Likewise, LE flux increases during the day with diurnal warming due to increase in ET, and usually the maximum precipitation peak occurs just after the maximum LE value, this due to the increase in condensation potential especially in the afternoon (Lieth & Werger,2012; Stuart et al., 2002).

The variation of the fluxes between seasons of the year (dry season, rainy season, MSD) is linked with precipitation. The main differences between 2020 and 2021 were observed in the MSD and the second part of the rainy season, where the CO_2 flux had an outstanding behavior, since, in this period, the trend towards positive values was greater than in 2020. Differences were observed in LE, H and CO_2 fluxes during the MSD, for which the year 2021 showed greater variability compared to the year 2020. Likewise, the greatest difference in the means was found in LE and CO_2, fluxes with higher values for 2021. It should be noted that the precipitation during the MSD of 2020 and 2021 was on average 0 mm, however, the MSD during 2020 had a longer duration.

When analyzing the precipitation at La Hilda (Mukherjee et al (2015) classification), a predominance of light-type events was observed, especially in the first part of the year and, the most important events categorized as heavy and very heavy increase in the second part of the year. The main modulators of these strong events, highlighted as events to be investigated in this study, were tropical waves and the migration of ITCZ, as well as hurricane Eta.

A relevant event was Hurricane Eta (November 2020), in which both energy flows and CO_2 presented a different behavior from the rest of the events. LE and CO_2 were practically constant and with values that tended to zero from the third to the fifth day of the event, because the indirect influence of this hurricane caused several days in a row of rainfall, which saturated the soils, which leads both ET and vegetation production are

almost constant (Chen et al.,2013; Carvalho Gomes et al., 2016). H flux also exhibited more variability during long events. This could be related with the change in temperature between surface and rainfall (Wei et al., 2014). Therefore, the variability of energy and mass fluxes is sensible to the amount and duration of the rainfall.

It was observed that the SWC remains practically constant, in the hours before the rainfall starts, this for the most important precipitation events, that is, it had a well-defined diurnal cycle. Once the rain starts, there is variation of the SWC with an increasing tendency. Likewise, in the case of Hurricane Eta, as it is a long-term event, with soil saturation, the SWC remains almost constant.

The behavior of the WUE in this study is consistent with other investigations, where it is observed that the intra-seasonal variability of the WUE is influenced by strong rain events, because these rain events affect the variability of surface fluxes. In addition, the same relationship with precipitation is observed between the dry and rainy seasons, where the driest months presented a lower WUE compared to the months of the rainy season. In addition, as with the surface fluxes, the WUE was affected by the influence of Hurricane Eta, where the values were very high compared to the other events. Finally, to explain the daily variability of the WUE, it is necessary to further investigate the influence of factors such as atmospheric conditions and plant status, since these affect ET and GPP.

When analyzing the sap flux for the different categories of precipitation, it was observed that it varies according to intensity, that is, for the lowest categories of rain, the greatest amount of data is concentrated in the lowest sap values, and for very strong events, the higher concentration of data moves to higher values.

Among the main recommendations are a more in-depth analysis of the relationship between sap flux and precipitation (for the different categories) and the possible physiological plant response that explains the behavior of these two variables. Likewise,

a more exhaustive investigation on the behavior of the fluxes during the MSD (LE, H, CO_2, ET and SWC) is necessary. Moreover, it is important to evaluate how energy fluxes, as well as with CO_2, SWC and sap fluxes behave, days after Hurricane Eta, due to its strong influence on these variables.

Finally, continue with the evaluation of the possible impact of intense rain events on the fluxes with the update of the data, and thus increase the sample and be able to generate more robust results. As well as, the analysis of the photosynthetically active radiation (PAR), since it is a variable of great importance when evaluating the variables analyzed here, due to its influence on the photosynthetic process.

Annex 1

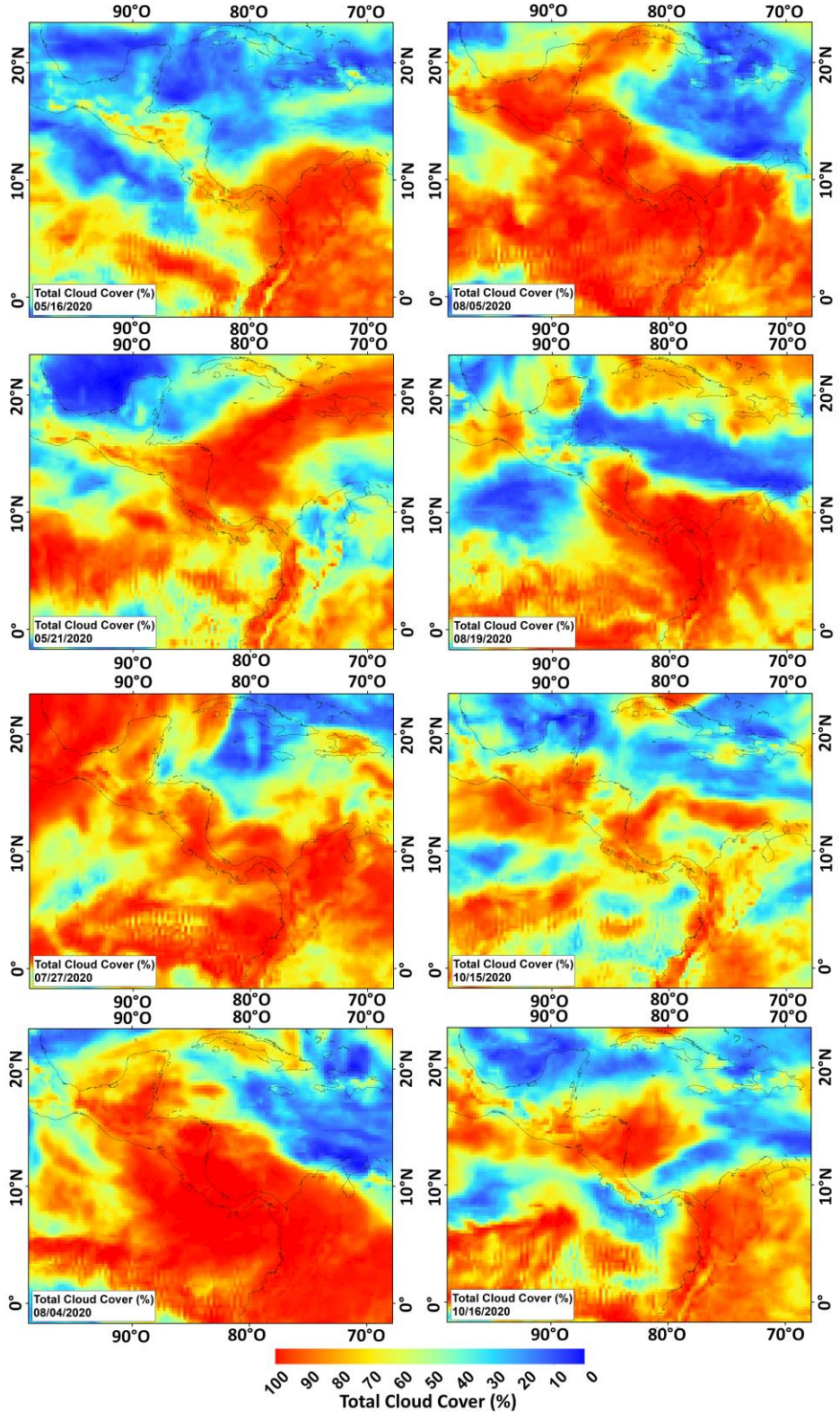

Figure A.1.1 *Maps of total cloud cover (%) for the events of 2020 in the Table 3.1. Red colors indicate 100% of cloud cover.*

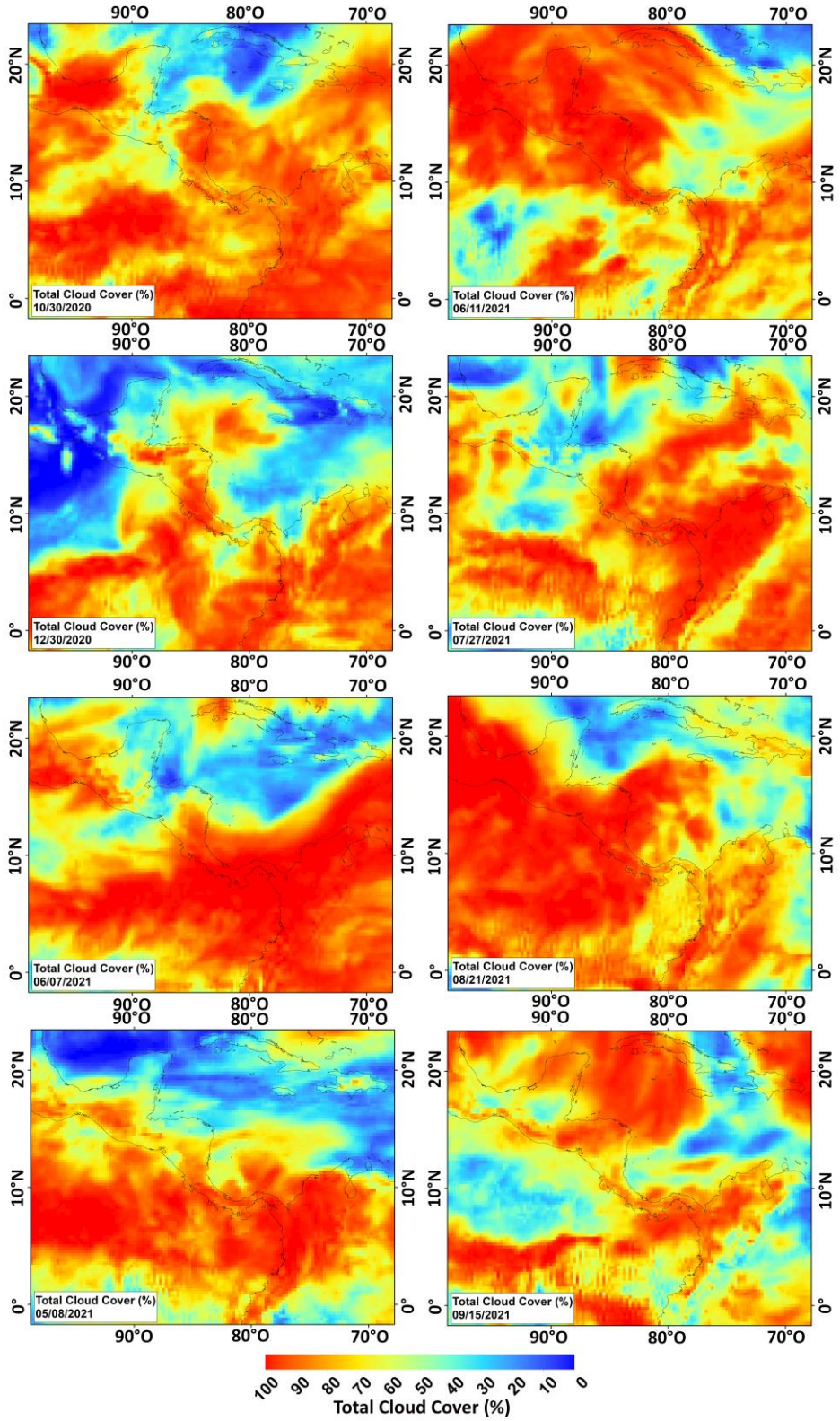

Figure A.1.2 *Maps of total cloud cover (%) for the events of 2020-2021 in the Table 3.1. Red colors indicate 100% of cloud cover (data: Reanalysis Era 5).*

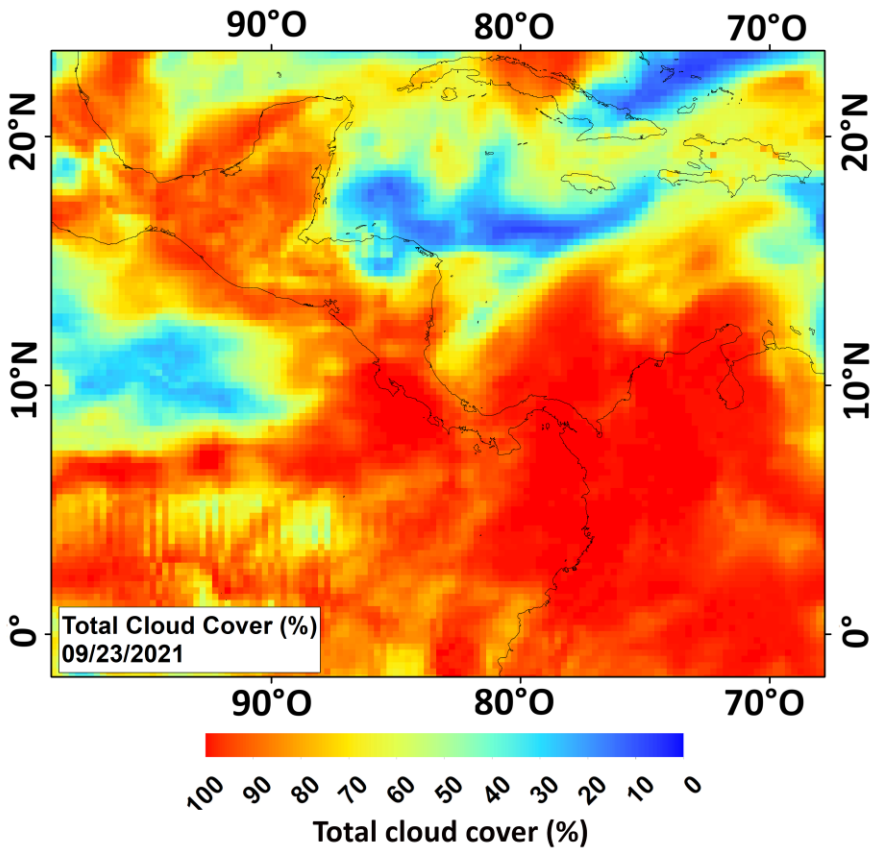

Figure A.1.3 *Map of total cloud cover (%) for the event on 09/23/2021 in Table 3.1. Red colors indicate 100% of cloud cover (data: Reanalysis Era 5).*

Annex 2

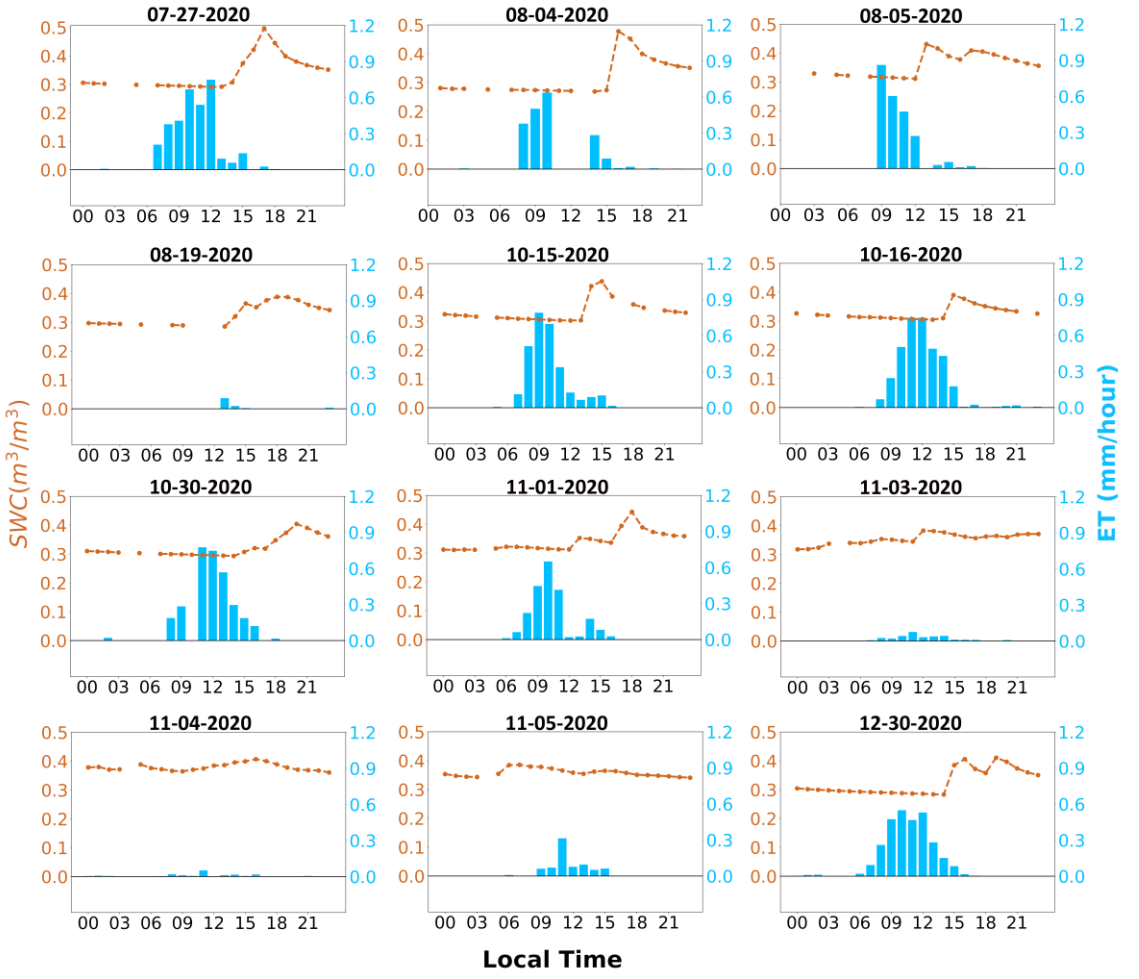

Figure A.2.1 *SWC diurnal cycle (orange line) and evapotranspiration (light-blue bars) for extreme rainfall events for 2020 at La Hilda (Table 2.3). November 2020 event is Hurricane Eta for which a different behavior of the SWC is observed with respect to rainfall compared to the other events.*

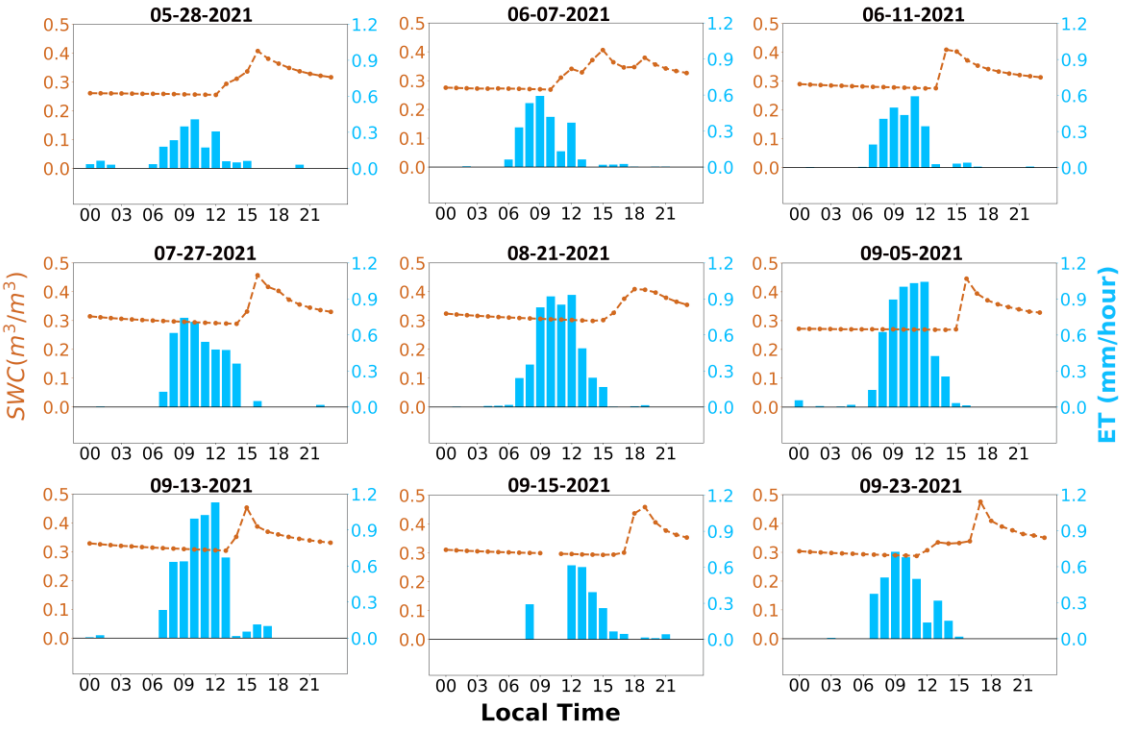

Figure A.2.2 *SWC diurnal cycle (orange line) and evapotranspiration (light-blue bars for extreme rainfall events for 2021 at La Hilda (Table 2.3).*

References

Allan et al. (2021). Climate Change 2021, The Physical Science Basis. *IPCC*. https://www.ipcc.ch/report/ar6/wg1/downloads/report/IPCC_AR6_WGI_Full_Report.pdf

Alpízar, M. et al. (2018). Estadísticas de comercio exterior de Costa Rica 2015. PROCOMER.

Ahrens, C. D., & Henson, R. (2009). Meteorology today: an introduction to weather, climate, and the environment. Cengage Learning.

Arredondo et al. (2018). Does precipitation affect soil respiration of tropical semiarid grasslands with different plant cover types? *Agriculture, Ecosystems & Environment*, 251, 218-225.

Baker, J. V., & Van Bavel, C. H. M. (1987). Measurement of mass flow of water in the stems of herbaceous plants.

Baldocchi, D. (1994). A comparative study of mass and energy exchange rates over a closed C3 (wheat) and an open C4 (corn) crop: II. CO2 exchange and water use efficiency. *Agricultural and Forest Meteorology*, 67(3-4), 291-321.

Bhatla, S. C., & Lal, M. A. (2018). Plant physiology, development and metabolism. Springer.

Bermingham, E. et al. (Eds.). (2005). Tropical rainforests: past, present, and future. University of Chicago Press.

Bonan, G. (2015). Ecological climatology: concepts and applications. Cambridge University Press.

Burba, G., & Anderson, D. (2010). A brief practical guide to eddy covariance flux measurements: principles and workflow examples for scientific and industrial applications. Li-Cor Biosciences.

Cabral, O. et al. (2013). Fluxes of CO2 above a sugarcane plantation in Brazil. *Agricultural and forest meteorology*, 182, 54-66.

Campbell, N.; Reece, J. (2007). *Biología* (7th ed.). Médica Panamericana.

Chapin III, F. S. et al. (2011). Principles of terrestrial ecosystem ecology. Springer Science & Business Media.

Chen, Z. et al. (2013). Temperature and precipitation control of the spatial variation of terrestrial ecosystem carbon exchange in the Asian region. *Agricultural and Forest Meteorology*, *182*, 266-276.

Calvo-Solano, O. D. et al. (2018). Impactos de las sequías en el sector agropecuario del Corredor Seco Centroamericano. *Agronomía Mesoamericana*, 29(3), 695-709.

Chinchilla-Soto, C. et al. (2021). Quantifying the Annual Cycle of Water Use Efficiency, Energy and CO2 Fluxes Using Micrometeorological and Physiological Techniques for a Coffee Field in Costa Rica. *Forests*, 12(7), 889.

Cooley, S.S. et al. (2019). Assessing regional drought impacts on vegetation and evapotranspiration: a case study in Guanacaste, Costa Rica. *Ecological Applications*, 29(2), p.e01834.

CPC. (2020). El Niño Southern Oscillation (ENSO) diagnostic discussion. Climate Prediction Center. https://www.cpc.ncep.noaa.gov/products/analysis_monitoring/enso_advisory/ensodisc.pdf

Campbell Scientific (2012). HFP01-L Soil Heat Flux Plate. Campbell Scientific.

Dai, A. et al. (1999). Effects of clouds, soil moisture, precipitation, and water vapor on diurnal temperature range. *Journal of Climate*, 12(8), 2451-2473.

Davin, E. L., & de Noblet-Ducoudré, N. (2010). Climatic impact of global-scale deforestation: Radiative versus nonradiative processes. *Journal of Climate*, *23*(1), 97-112.

de Carvalho Gomes, L. et al. (2016). Trees modify the dynamics of soil CO2 efflux in coffee agroforestry systems. *Agricultural and Forest Meteorology*, *224*, 30-39.

Durán-Quesada, A. M. et al. (2017). Role of moisture transport for Central American precipitation. *Earth System Dynamics*, *8*(1), 147-161.

Durán-Quesada, A. M. et al. (2020). Climate perspectives in the intra–Americas seas. *Atmosphere*, 11(9), 959.

Dynamax (2007). Dynagage Sap Flow Sensor, User Manual. Dynamax.

Fahad, S. et al. (2017). Crop production under drought and heat stress: plant responses and management options. *Frontiers in plant science*, *8*, 1147.

FAO. (2015). World Programme for the Census of Agriculture 2020: Volume 1- Programme, concepts and definitions.

Foken, T., & Napo, C. (2008). Micrometeorology (Vol. 2). Berlin. Springer.

Gimenez et al. (2005). Plant-Water Relations. Elseiver.

Gu, C. et al. (2021). Discrepant responses between evapotranspiration-and transpiration-based ecosystem water use efficiency to interannual precipitation fluctuations. *Agricultural and Forest Meteorology*, 303, 108385.

Harper, C. W. et al. (2005). Increased rainfall variability and reduced rainfall amount decreases soil CO_2 flux in a grassland ecosystem. *Global Change Biology*, *11*(2), 322-334.

Hidalgo, H.G. et al. (2019). Precursors of quasi-decadal dry-spells in the Central America Dry Corridor. *Climate Dynamics*, *53*(3), pp.1307-1322.

Holton, J. R. (2004). An introduction to dynamic meteorology. *American Journal of Physics*, 41(5), 752-754.

Huxman, T. E. et al. (2004). Precipitation pulses and carbon fluxes in semiarid and arid ecosystems. *Oecologia*, *141*(2), 254-268.

IMN (2020). Clima y las Regiones Climáticas. *Instituto Meteorológico Nacional*. https://www.imn.ac.cr/clima-en-costa-rica

IMN (2021a). El ENOS y sus efectos sobre Costa Rica. *Instituto Meteorológico Nacional*. https://www.imn.ac.cr/en/enos

IMN. (2021b). Boletín ENOS. *Instituto Meteorológico Nacional*. https://www.imn.ac.cr/boletin-enos.

INEC (2015). VI Censo Nacional Agropecuario: Resultados Generales. Costa Rica. *Instituto Nacional de Estadística y Censos.*

Jia, J. et al. (2016). Response of forestland soil water content to heavy rainfall on Beijing Mountain, northern China. *Journal of Forestry Research*, *27*(3), 541-550.

Kipp & Zonen (2014). CNR 4 Net Radiometer, Instruction Manual. *Kipp & Zonen.*

Kleidon, A. (2018). Encyclopedia of Ecology, Energy Balance (2nd ed., Vol. 4). Elsevier.

Krishnan, P. et al. (2012). Energy exchange and evapotranspiration over two temperate semi-arid grasslands in North America. *Agricultural and Forest Meteorology*, 153, 31-44.

Lal, R. (2004). Agricultural activities and the global carbon cycle. *Nutrient cycling in agroecosystems*, *70*(2), 103-116.

Lee et al. (Eds.). (2004). Handbook of micrometeorology: a guide for surface flux measurement and analysis (Vol. 29). Springer Science & Business Media.

Lei, N., & Han, J. (2020). Effect of precipitation on respiration of different reconstructed soils. *Scientific reports*, 10(1), 1-10.

Li, X. et al. (2019). A simple and objective method to partition evapotranspiration into transpiration and evaporation at eddy-covariance sites. *Agricultural and Forest Meteorology*, *265*, 171-182.

Li-Cor (2016a). EDDY PRO Software, Instruction Manual. Li-Cor Biosciences.

Li-Cor (2016b). Li7200RS Enclosed CO2 /H2O Gas Analyzer, Instruction Manual. *Li-Cor Biosciences*.

LiCor (2019a). Li-200R Pyranometer, Instruction Manual. *Li-Cor Biosciences*.

LiCor (2019b). Terrestrial Quantum Sensors, Instruction Manual. *Li-Cor Biosciences*.

Li-Cor (2020). LI7200RS Enclosed CO2 /H2O Analyzer. https://www.licor.com/env/products/eddy_covariance/LI-7200RS.html

Lieth, H., & Werger, M. J. (Eds.). (2012). Tropical rainforest ecosystems: biogeographical and ecological studies.

Magaña, V. et al. (1999). The midsummer drought over Mexico and Central America. Journal of Climate, 12(6), 1577-1588.

Maldonado, T. et al. (2018). A review of the main drivers and variability of Central America's Climate and seasonal forecast systems. *Revista de Biología Tropical*, 66(1-1), S153-S175.

Mares, M. A. (2017). *Encyclopedia of deserts*. University of Oklahoma Press.

Martin, E. R., & Schumacher, C. (2011). Modulation of Caribbean precipitation by the Madden–Julian oscillation. *Journal of Climate*, 24(3), 813-824.

Mölders, N., & Kramm, G. (2014). Lectures in meteorology (pp. 1-591). Berlin: Springer

Mora, S. (2019). Informe comercio exterior del Sector Agropecuario. I trimestre 2018-2019. SEPSA.

Mora, S. & Quirós, Y. (2019). Boletín Estadístico Agropecuario N.29. Serie Cronológica 2015-2018. SEPSA.

Mukherjee, S. et al. (2016). Investigation of dominant modes of monsoon ISO in the northwest and eastern Himalayan region. *Theoretical and Applied Climatology*, 125(3), 489-498.

Nair, K. P. (2010). The agronomy and economy of important tree crops of the developing world.

NOAA. (2020). Record-breaking Atlantic hurricane season draws to an end. National Oceanic and Atmospheric Administration. https://www.noaa.gov/media-release/record-breaking-atlantic-hurricane-season-draws-to-end

Olchev, A. et al. (2015). Response of CO_2 and H_2O fluxes of a mountainous tropical rain forest in equatorial Indonesia to El Niño events. *Biogeosciences Discussions*, 12(6), 4405-4431.

Pascale, S. et al. (2021). Natural variability vs forced signal in the 2015–2019 Central American drought. *Climatic Change*, 168(3), pp.1-21.

Pasch et al. (2021). Hurricante ETA. National Hurricane Center Tropical Cyclone Report. https://www.nhc.noaa.gov/data/tcr/AL292020_Eta.pdf

Samper, M., & Peters, G. (2001). Café de Costa Rica: un viaje a lo largo de su historia (No. 633.7389 S192). *Instituto del Café de Costa Rica, San José* (Costa Rica).

Perugini, L. et a. (2017). Biophysical effects on temperature and precipitation due to land cover change. *Environmental Research Letters*, *12*(5), 053002.

Ramírez, P. (1983). Estudio meteorológico de los veranillos en Costa Rica (No. P40/2161). (Costa Rica)].

Sakuratani, T. (1981). A heat balance method for measuring water flux in the stem of intact plants. *Journal of Agricultural Meteorology*, 37(1), 9-17.

Sánchez-Murillo, R. et al. (2017). Tropical precipitation anomalies and d-excess evolution during El Niño 2014-16. *Hydrological Processes*, *31*(4), pp.956-967.

Sharma, B. et al. (2015). Water use efficiency in agriculture: Measurement, current situation and trends (No. 612-2016-40604).

SHIKLOMANOV, Igor Alekseevich (ed.) (2009). The hydrological cycle. Eolss Publishers Company Limited.

Stevens (2018). HydraProbe Soil Sensor, User's Manual. Stevens.

Stewart, I.T. et al. (2022). Recent evidence for warmer and drier growing seasons in climate sensitive regions of Central America from multiple global datasets. *International Journal of Climatology*, 42(3), pp.1399-1417.

Timm, A., et al. (2014). Energy partitioning and evapotranspiration over a rice paddy in Southern Brazil. *Journal of Hydrometeorology*, 15(5), 1975-1988.

Texas Electronics (2017). Rain Gauge Tipping Bucket, TR-525M. Texas Electronics.

Torres, G. et al. (2021). Coffea arabica L: History, phenology and climatic aptitude of the state of São Paulo, Brazil. Arquivos do Instituto Biológico, 88.

Vaisala (2012). HMP155 Humidity and Temperature Probe. Vaisala.

Van Kanten, R., & Vaast, P. (2006). Transpiration of arabica coffee and associated shade tree species in sub-optimal, low-altitude conditions of Costa Rica. *Agroforestry Systems*, 67(2), 187-202.

Wei, J., & Dirmeyer, P. A. (2019). Sensitivity of land precipitation to surface evapotranspiration: A nonlocal perspective based on water vapor transport. *Geophysical Research Letters*, *46*(21), 12588-12597.

Wei, N. et al. (2014). Impact of precipitation-induced sensible heat on the simulation of land-surface air temperature. *Journal of Advances in Modeling Earth Systems*, 6(4), 1311-1320.

Wilfred, V. (2008). Genetic improvement of bioenergy crops. Springer.

Wu, C. et al. (2013). Positive impacts of precipitation intensity on monthly CO2 fluxes in North America. *Global and Planetary Change*, *100*, 204-214.

Xiao, J. et al. (2010). A continuous measure of gross primary production for the conterminous United States derived from MODIS and AmeriFlux data. *Remote sensing of environment*, 114(3), 576-591.

Xiao, J. et al. (2013). Carbon fluxes, evapotranspiration, and water use efficiency of terrestrial ecosystems in China. *Agricultural and Forest Meteorology*, 182, 76-90.

Yuan, M. et al. (2021). Global response of terrestrial gross primary productivity to climate extremes. *Science of the Total Environment*, 750, 142337.